



MT-DAO: Multi-timescale Distributed Adaptive Optimizers with Local Updates

Alex Iacob^{†,1,2} Andrej Jovanović^{*,1} Mher Safaryan^{*,3} Meghdad Kurmanji¹

Lorenzo Sani^{1,2} Samuel Horváth⁴ William F. Shen¹ Xinchu Qiu¹

Nicholas D. Lane^{1,2}

Abstract

Training large models with distributed data parallelism (DDP) requires frequent communication of gradients across workers, which can saturate bandwidth. *Infrequent* communication strategies (e.g., Local SGD) reduce this overhead but, when applied to adaptive optimizers, often suffer a performance gap relative to *fully synchronous* DDP. We trace this gap to a time-scale mismatch: the optimizer’s fast-moving momentum, tuned for frequent updates, decays too quickly to smooth gradients over long intervals, leading to noise-dominated optimization. To address this, we propose MT-DAO, a family of optimizers that employs multiple slow- and fast-moving first momenta or the gradient to track update dynamics across different time scales, for which we provide the first convergence guarantees. Empirically, for language-model pre-training, this eliminates the performance gap with DDP, outperforming infrequent-communication baselines in perplexity and reducing iso-token wall-clock time relative to DDP by 6–27% on Ethernet interconnects. At the 720M scale, MT-DAO reaches a target perplexity in 24% fewer steps and 35% less time than the single-momentum DDP baseline. MT-DAO enables effective cross-datacenter training and training over wide geographic areas.

1 Introduction

The scalability of training infrastructure is impeded by the communication required for Distributed Data Parallelism (DDP). Infrequent parameter-averaging strategies like Local SGD [51] reduce this overhead, yet extensions to adaptive optimizers [10, 7] show a performance gap relative to DDP [46, 7]. Charles et al. [7] finds that infrequent averaging, even with Nesterov momentum at round boundaries [43], underperforms DDP for models up to 2.4B parameters and worker counts exceeding 2.

We hypothesize this gap stems from a *timescale mismatch*. Optimizers use fast-moving momenta (low $\beta_1 \approx 0.9$) that smooth high-frequency noise under DDP but *decay too rapidly* between infrequent synchronizations. This decay prevents a stable shared trajectory, leading to our central question:

Can a distributed adaptive optimizer with β ’s suited for infrequent communication close the performance gap with DDP while providing convergence guarantees?

We propose MT-DAO, which brings multi-momentum optimizers [36, 40] to the distributed, infrequent-communication regime. MT-DAO resolves the mismatch by using slow-moving momenta (e.g., $\beta \approx 0.999$) to preserve trajectory information across synchronizations while remaining responsive via a fast momentum. In its simplest quasi-hyperbolic form [37], MT-DAO uses the current

[†]aai30@cam.ac.uk; ^{*}Equal contributions; ¹University of Cambridge; ²Flower Labs; ³Institute of Science and Technology Austria; ⁴Mohamed bin Zayed University of Artificial Intelligence

gradient as the fast momentum, adds no memory or communication overhead, and requires only one additional hyperparameter. Crucially, unlike methods that use a momentum-based outer optimizer [43, 12] at synchronization boundaries, MT-DAO needs **no extra memory buffers** or multiple outer hyperparameters.

Empirically, slow momentum acts as a regularizer, improving update alignment by increasing cosine similarity between worker pseudo-gradients [43]. This stability lets MT-DAO improve perplexity over low-communication baselines. Furthermore, MT-DAO matches or exceeds its DDP analogue at larger scales, **closing the perplexity gap** for models up to 720M parameters.

Contributions :

1. **A Provably Convergent Multi-Timescale Framework.** We introduce MT-DAO, the first framework to integrate multi-momentum strategies into distributed settings, with convergence guarantees for heterogeneous momentum timescales and synchronization frequencies.
2. **Closing the Performance Gap Efficiently.** MT-DAO matches synchronous DDP, outperforming baselines in perplexity, reducing wall-clock time by 6–27%; at 720M it reaches a target perplexity in 24% fewer steps and 35% less time than a DDP baseline.
3. **Noise Suppression and Information Retention.** MT-DAO’s slow momentum preserves mutual information across rounds and reduces inter-worker momentum variance.
4. **Resilience to Infrequent Communication.** MT-DAO lowers the rate of change of parameters and momenta, improving tolerance to low communication frequencies.
5. **Alignment of Worker Trajectories.** MT-DAO increases cosine similarity of local worker update trajectories, which reduces worker drift and aligns the overall model update.

2 Multi-timescale Distributed Adaptive Optimizers (MT-DAO)

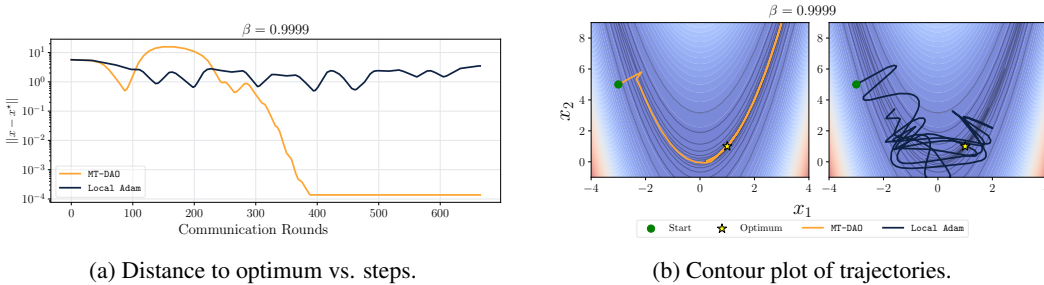


Figure 2: To highlight the stability benefit of MT-DAO, we illustrate its performance on a toy non-convex problem. Crucially, under a high momentum decay of $\beta = 0.9999$, prior stateful methods like Local Adam [10] become unstable and fail to converge, whereas MT-DAO maintains its rapid and stable convergence. We optimize the non-convex Rosenbrock function $f(x_1, x_2) = (1 - x_1)^2 + 100(x_2 - x_1^2)^2$ with $M = 256$ workers and IID Gaussian noise ($\sigma = 2$).

Our analysis begins by characterizing the conflict between optimizer momentum timescales and the long communication intervals of infrequent-communication training. We consider the standard setting. Let M be the total number of workers and K be the number of local updates performed by each worker per round. The goal is to minimize a global objective $f(x) := \frac{1}{M} \sum_{m=1}^M f_m(x)$ over the model parameters x , where each $f_m(x)$ is the local objective $\mathbb{E}_{\xi \sim \mathcal{D}_m} [F_m(x; \xi)]$ for a data sample ξ drawn from data distribution \mathcal{D}_m . We posit that the performance degradation in this regime stems from a fundamental mismatch between the optimizer’s memory and the communication period.

2.1 Timescale Mismatch

The first momentum in adaptive optimizers is an Exponential Moving Average (EMA). Let u_t be the momentum, β be the momentum decay factor, and g_t be the gradient at step t . The momentum is then given by $u_t = \beta u_{t-1} + (1 - \beta)g_t$. Its effective memory is quantified by its half-life,

$\tau_{0.5}(\beta) = \frac{\ln 0.5}{\ln \beta}$, the number of steps until the momentum decays by 50% [40]. A typical $\beta_1 = 0.9$ yields $\tau_{0.5} \approx 6.6$ steps, suitable for frequent communication. A conflict arises when $K \gg \tau_{0.5}$, common in communication-efficient training ($K \in [32, 512]$). Unrolling the momentum update over K local steps from a synchronized state u_t gives: $u_{t+K} = \beta^K u_t + (1 - \beta) \sum_{k=0}^{K-1} \beta^k g_{t+K-k}$. The influence of the global state u_t on the final local state u_{t+K} decays with β^K . For $\beta_1 = 0.9$ and $K = 32$, this factor is negligible (≈ 0.03). In such a setting, the worker becomes reliant on high-variance, potentially biased local gradients. For example, if noise is independent across workers, the variance of the final local momentum is $\text{Var}(u_{t+K}) = \frac{1-\beta}{1+\beta} (1 - \beta^{2K}) \sigma_m^2$ (see Section F), with σ_m^2 being the gradient variance of worker m . As $\beta \rightarrow 1$ the factor $\frac{1-\beta}{1+\beta}$ suppresses variance. For $\beta \rightarrow 0$, variance approaches σ_m^2 , exposing local updates to noise-induced instability.

An alternative interpretation of this memory decay is offered by information theory, which quantifies the preserved signal between the initial global momentum U_t and the final local momentum U_{t+K} via their mutual information, $I(U_{t+K}; U_t)$. By modeling the local updates as a linear process $U_{t+K} = \beta^K U_t + L$, where L is the accumulated local gradient noise, a closed-form expression can be derived when assuming Gaussian distributions for the states and noise with covariances Σ_{U_t} and Σ_L respectively. The mutual information is $I(U_{t+K}; U_t) = \frac{1}{2} \log \det(I + \beta^{2K} \Sigma_{U_t} \Sigma_L^{-1})$ (see Section F). As $\beta^K \rightarrow 0$, mutual information vanishes, implying statistical independence with respect to the momentum at the start of the interval. As $\beta^K \rightarrow 1.0$, the initial signal is preserved.

2.2 The Challenge of High- β Optimizers

Although both arguments above encourage the use of large β values as a solution to this timescale mismatch problem, previous work has shown that high-momentum optimizers are often unfeasible in practice [36]. Without modification, they are insufficiently responsive to changes in the loss landscape and are prone to oscillations (see the top of Fig. 3), yielding subpar performance.

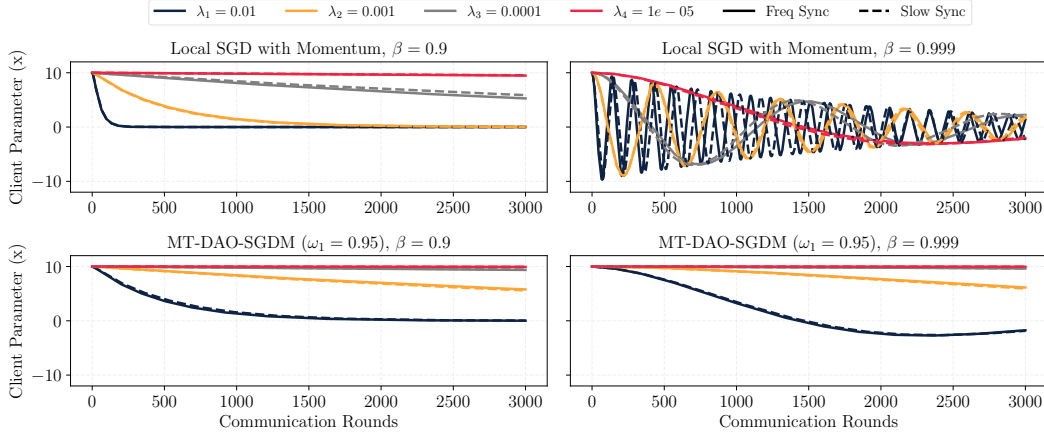


Figure 3: Comparison of Local SGDM with standard momentum (**top**) and MT-DAO-SGDM ($N = 1$ momentum, $\omega_1 = 0.95$) (**bottom**) for the function $f(x; \lambda) = \frac{1}{2} \lambda x^2$ with $x \in \mathbb{R}$ for various parameters controlling the rate of change λ and sync frequencies (frequent: solid, infrequent/slow: dashed). While both optimizers are stable at low momentum ($\beta = 0.9$), at high momentum ($\beta = 0.999$) Local SGD with standard momentum becomes unstable for high λ while MT-DAO-SGDM remains stable.

This instability motivates using multi-momentum methods [36, 37, 40]. Such methods compose the optimizer update as a linear combination of slow and fast-moving first momenta, or the gradient in the case of Quasi-hyperbolic methods [37]. This avoids common pitfalls of high-momentum methods by responding to changes in the loss landscape via the fast momentum/gradient. Recent works [40, 49] have shown that such optimizers can provide SOTA results, outperforming popular optimizers such as Adam [35], Muon [20], and Dion [1].

Algorithm 1 MT-DAO-Adam, local bias correction omitted to save space.

Require: Model tensors, hyper-parameters

- 1: $x_0 \in \mathbb{R}^d, \{\bar{u}_{-1}^j\}_{j=1}^N \in (\mathbb{R}^d)^N, \bar{v}_{-1} \in \mathbb{R}^d$ — initial params, N first momenta, second momentum
 - 2: $\{\beta_{1,j}\}_{j=1}^N, \beta_2 \in [0, 1)$ — decay rates for each momentum state
 - 3: $\{\omega_j\}_{j=1}^N \in [0, 1]$ — convex combination coefficients for first momenta, $\sum_{j=1}^N \omega_j \leq 1.0$
 - 4: $\rho \in \mathbb{R}_+, \{\eta_t\}_{t=0}^{T-1}$ — clipping radius, learning-rate schedule
 - 5: $T, M \in \mathbb{N}_+$ — total optimization steps and number of workers
 - 6: $K_x, \{K_j\}_{j=1}^N, K_v \in (\mathbb{N}_+)^{N+2}$ — communication periods for parameters and states
 - 7: `OuterOpt` : $\mathbb{R}^d \rightarrow \mathbb{R}^d$ — update params using an outer optimizer, averaging by default
- Ensure:** $x_T, \{u_{T-1}^j\}_{j=1}^N, v_{T-1}$
- 8: **for each worker** m : initialize $x_0^m, \{u_{-1}^{j,m}\}, v_{-1}^m$
 - 9: **for** $t = 0, \dots, T - 1$ **do**
 - 10: **for all workers** $m = 0, \dots, M - 1$ **in parallel do**
 - 11: $\hat{g}_t^m \leftarrow \text{clip}(\nabla F(x_t^m; \xi_t^m), \rho)$ clipped stochastic gradient
 - 12: **for** $j = 1$ **to** N **do** update N first momenta
 - 13: $u_t^{j,m} \leftarrow \beta_{1,j} \bar{u}_{t-1}^j + (1 - \beta_{1,j}) \hat{g}_t^m$
 - 14: $\bar{u}_{t-1}^j \leftarrow \text{if } (t \bmod K_j = 0) \text{ then } \mathbb{E}_m[u_{t-1}^{j,m}] \text{ else } u_{t-1}^{j,m}$ sync u^j every K_j steps
 - 15: $v_t^m \leftarrow \beta_2 \bar{v}_{t-1} + (1 - \beta_2)(g_t^m)^2$
 - 16: $\bar{v}_{t-1} \leftarrow \text{if } (t \bmod K_v = 0) \text{ then } \mathbb{E}_m[v_{t-1}^m] \text{ else } v_{t-1}^m$ sync v every K_v steps
 - 17: $\Delta_t^m \leftarrow \frac{1}{\sqrt{v_t^m + \epsilon}} \left[(1 - \sum_{j=1}^N \omega_j) \hat{g}_t^m + \sum_{j=1}^N \omega_j u_t^{j,m} \right]$ form combined update direction
 - 18: $x_{t+1}^m \leftarrow \bar{x}_t - \eta_t \Delta_t^m$
 - 19: $\bar{x}_t \leftarrow \text{if } (t \bmod K_x = 0) \text{ then } \text{OuterOpt}(\mathbb{E}_m[x_t^m]) \text{ else } x_t^m$ sync x every K_x steps
-

2.3 The MT-DAO Method and Algorithm

Based on this analysis, we formalize the MT-DAO framework in Algorithm 1 for Adam with a variant for ADOPT in Algorithm 2 and one for SGD with Momentum (SGDM) presented in Algorithm 3. It accommodates adaptive optimizers with N first-order momenta $\{u^j\}$ and a single second-order momentum v . The parameter update is driven by a convex combination with hyper-parameters $\{\omega_j\}$ of these N preconditioned momenta and the preconditioned current gradient, which receives the remaining weight $1 - \sum_{j=1}^N \omega_j$. We highlight these additions in purple. This inclusion of the current gradient term effectively implements the Quasi-hyperbolic Momentum (QHM) structure within this generalized multi-momentum framework. The `OuterOpt` procedure represents arbitrary parameter optimizers such as Federated Averaging [39], Nesterov Momentum [18], or FedOPT [43]. Unless stated otherwise, our analysis and arguments refer to using averaging to align with previous convergence analyses [10, 19]. MT-DAO-Adam reduces communication costs by $(\frac{1}{K_x} + \sum_{j=1}^N \frac{1}{K_j} + \frac{1}{K_v})^{-1}$ over DDP.

This generalized framework recovers previous distributed adaptive optimizers [51, 12, 10, 19]. It also introduces **the first-ever formulations for provably convergent distributed variants of multi-momentum optimizers** [36, 37, 40]. Figure 3 (bottom) shows an example of MT-DAO-SGDM converging for both high and low β_1 with a quasi-hyperbolic formulation while the Local SGD with momentum averaging method fails for high β_1 . To highlight the stability of MT-DAO-Adam, Figure 2 illustrates its convergence on a common toy non-convex problem [40] under high momentum ($\beta = 0.9999$), a setting where prior provably convergent methods like Local Adam [10] become unstable and do not reach the optimum.

3 Convergence Guarantees for MT-DAO

This section provides a theoretical convergence analysis for the proposed MT-DAO approach using the SGDM optimizer. The analysis, detailed in Section D, relies on the following standard assumptions.

Assumption 1 (Lower bound and smoothness). *The overall loss function $f: \mathbb{R}^d \rightarrow \mathbb{R}$ is lower bounded by some $f^* \in \mathbb{R}$ and all local loss functions f_m are L -smooth:*

$$\|\nabla f_m(x) - \nabla f_m(y)\| \leq L\|x - y\|, \quad \text{for any } x, y \in \mathbb{R}^d.$$

Assumption 2 (Unbiased noise with bounded stochastic variance). *The stochastic gradient g^m of local loss function f_m computed by machine m is unbiased and the noise has bounded variance:*

$$\mathbb{E}[g^m] = \nabla f_m(x), \quad \mathbb{E}[\|g^m - \nabla f_m(x)\|^2] \leq \sigma^2, \quad \text{for any } x \in \mathbb{R}^d.$$

Assumption 3 (Bounded heterogeneity). *For any $x \in \mathbb{R}^d$, the heterogeneity is bounded by*

$$\frac{1}{M} \sum_{m=1}^M \|\nabla f_m(x)\|^2 \leq G^2 + B^2 \|\nabla f(x)\|^2.$$

These are standard assumptions in smooth non-convex optimization [59, 24, 56, 60], covering homogeneous data as a special case ($G^2 = 0, B^2 = 1$). For analytical tractability, we model periodic synchronization every K steps as a probabilistic event. Model parameters are averaged with probability $p_x = 1/K_x$, the j -th momentum is averaged with probability $p_j = 1/K_j$. The gradient is treated as a momentum with $\beta = 0$.

Theorem 1. *Let Assumptions 1, 2 and 3 hold. Then, choosing the step size $\eta = \min(\eta_0, \frac{1}{\sqrt{T}})$ where $\eta_0 \stackrel{\text{def}}{=} 1/(4L \max(\beta_\omega, 6\sqrt{\psi \max(1, B^2 - 1)}))$ with constants*

$$\beta_\omega \stackrel{\text{def}}{=} \sum_{j=1}^N \frac{\omega_j \beta_j}{1 - \beta_j}, \quad \text{and} \quad \psi \stackrel{\text{def}}{=} \frac{4(1 - p_x)}{p_x^2} \sum_{j=1}^N \omega_j \frac{(1 - \beta_j)(1 - p_j)}{1 - (1 - p_j)\beta_j} \quad (1)$$

the average iterates $x_t = \mathbb{E}_m[x_t^m]$ of MT-DAO-SGDM converge with the following rate:

$$\frac{1}{T} \sum_{t=0}^{T-1} \mathbb{E} \|\nabla f(x_t)\|^2 \leq \frac{4}{\sqrt{T}} \left(f(x_0) - f^* + \frac{L\sigma^2}{2M} \right) + \mathcal{O} \left(\frac{1 + \beta_\omega^2 + \psi}{T} \right). \quad (2)$$

The derived bound in (2) achieves the optimal $\mathcal{O}(1/\sqrt{T})$ asymptotic rate for smooth non-convex stochastic optimization [5]. Distributed factors, such as client drift and data heterogeneity, are contained within the step-size constraint and the higher-order $\mathcal{O}(1/T)$ term, thus not affecting the asymptotic rate. The step size η is constrained by β_ω and ψ . The dependence $\psi = \mathcal{O}(1/p_x^2)$ shows that model synchronization frequency p_x is critical. The impact of momentum synchronization is nuanced: reducing a momentum's sync frequency p_j increases its contribution to ψ , but this is modulated by its decay rate β_j . This implies "slower" momenta (larger β_j) are more robust to infrequent synchronization. **This analysis reveals a trade-off: large β_j values constrain the step size via β_ω but reduce the communication penalty in ψ .** Furthermore, synchronizing only the model always (i.e., $p_x = 1, p_j = 0$) is algorithmically equivalent to synchronizing only the momenta always (i.e., $p_x = 0, p_j = 1$). In the boundary case where only model parameters are synced ($p_x = 1, p_j = 0$), $\psi = 0$ and the rate recovers that of mini-batch SGD [34].

4 Experimental Design

Building on our analysis, our experimental design answers the following research questions:

- RQ1** Does MT-DAO reduce momentum noise and preserve mutual information, as predicted?
- RQ2** Does MT-DAO better preserve task performance when decreasing communication frequency?
- RQ3** How does MT-DAO perform against DDP and prior communication-efficient optimizers?
- RQ4** How does slow momentum affect local optimization trajectories between synchronizations?

4.1 Setup

Models and Data. We use peri-norm [25] GPT-style transformer models of 16M, 125M, and 720M parameters (Table 2). The 16M model is used for hyperparameter sweeps and qualitative investigations, while the 125M and 720M models are used for scaling experiments and baseline comparisons. All models are trained with a sequence length of 2048 on the SmoLLM2 mixture [4]. We evaluate all models (16M, 125M, 720M) using validation perplexity on a held-out 10% portion of the training mixture. For further details, please see Section B.

Optimizers and Tuning Methodology. We use the ADOPT optimizer, a variant of Adam whose convergence rate is independent of the second-momentum decay rate β_2 and preserves performance [54]; we fix $\beta_2 = 0.9999$ to isolate the first momentum dynamics (governed by β_1 and ω). We use the CompleteP parameterization for one-shot transfer of the learning rate (LR) from small to large

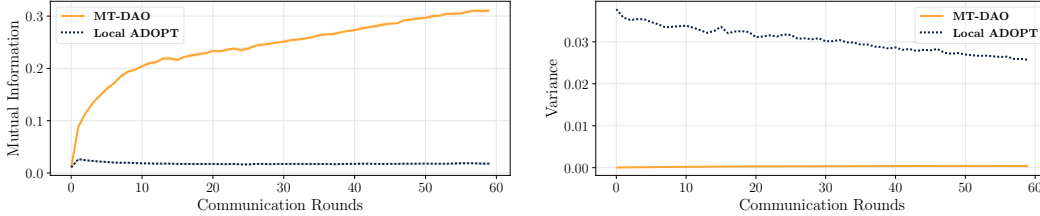


Figure 4: A comparison of MT-DAO ($\beta_1 = 0.999$) versus a Local ADOPT baseline ($\beta_1 = 0.95$) with a communication frequency of $K = 32$. For each communication round, we plot metrics computed between the momentum at the start (t) and end ($t + K$) of the round. MT-DAO’s slow momentum **preserves mutual information**, $I(U_t; U_{t+K})$, across rounds while the baseline’s momentum decays losing the global optimization direction (left). Furthermore, MT-DAO **reduces inter-worker momentum variance**, $\text{Var}(u_{t+K})$, indicating greater stability against local noise (right).

models [11]. For each combination of convex coefficients (ω ’s) and momentum decays (β ’s), we tune the learning rate on the 16M model and transfer the optimal hyperparameters to larger models directly without ever re-tuning (ω ’s) and (β ’s). To establish strong DDP baselines, we tune ω, β_1 parameters in the DDP setting and reuse them for MT-DAO. For complete details see Section B.2. We always use quasi-hyperbolic MT-DAO ($N = 1$) which does not require additional memory and reduces comms costs by $(\frac{1}{K_x} + \frac{1}{K_1} + \frac{1}{K_v})^{-1}$ over DDP.

Baselines. We compare MT-DAO against: the base optimizer (ADOPT) with DDP and DDP analogues to MT-DAO such as Quasi-hyperbolic Momentum (QHM) [37]. For communication-efficient baselines we use the provably convergent and stateful Local Adam [10] approach. We also compare against using Nesterov momentum as the outer optimizer [7]. We evaluate ML performance for communication-efficient methods under the same, fixed synchronization frequency. Unless otherwise stated we use $K = K_x = K_1 = K_v = 32$ steps, based on prior work finding a practical balance of performance efficiency [7]. We split the dataset in an IID fashion across 4 workers using 1 H100 per worker.

Other Metrics We analyze flattened models/momenta $s_t \in \mathbb{R}^d$ using several metrics. The **relative change** over K steps is measured as $\|s_{t+K} - s_t\|_2 / \|s_t\|_2$. To quantify the dispersion among M worker vectors, we compute the **cross-worker variance**, defined as $\frac{1}{M} \sum_{m=1}^M \|s_m - \bar{s}\|_2^2$. The statistical dependency between two random vectors at different timesteps is captured by their **mutual information**, $I(U_{t+K}; U_t)$. Finally, we measure alignment between vectors using **cosine similarity**.

5 Evaluation

This section empirically validates MT-DAO, showing its slow momentum preserves information and aligns workers (Sections 5.1 and 5.4), which improves stability under infrequent communication (Section 5.2) and allows it to close the performance gap with DDP at scale (Section 5.3).

5.1 MT-DAO Reduces Momentum Noise and Preserves Mutual Information (RQ1)

We now empirically validate the motivation of MT-DAO. Our results in Fig. 4 demonstrate that the slow-momentum of MT-DAO both preserves information about the global optimization direction across communication rounds and suppresses the variance induced by local updates.

Slow Momentum Is Preserved: The slow momentum in MT-DAO preserves its direction across communication rounds. This directional memory also reduces the influence of local gradient noise, leading to lower momentum variance across workers and **a more stable optimization path**.

5.2 MT-DAO Is Resilient to Infrequent Communication (RQ2)

We now investigate if MT-DAO provides greater resilience against infrequent synchronization, as predicted by our analysis in Section 3 showing that reducing the communication frequency of momenta with higher β has a diminished impact on the step size.

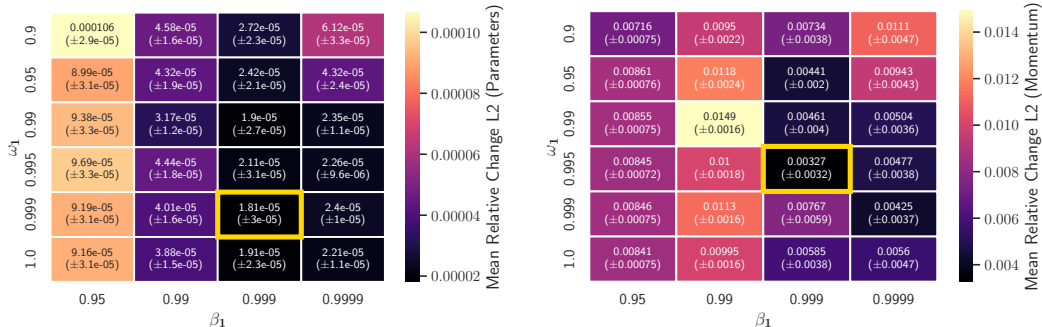


Figure 5: Mean relative L2 change and standard deviation across communication rounds of (left) model parameters and (right) the first momentum state, as a function of momentum decay (β_1) and weight (ω_1). In both cases, MT-DAO shows a significantly **reduced** relative rate of change with high (β_1, ω_1) (minimum in gold), which **reduces worker drift and thus makes parameter averaging more effective**. Each point on the grid corresponds to a configuration evaluated with its own independently tuned learning rate. Local ADOPT corresponds to ($\beta_1 = 0.95, \omega_1 = 1.0$).

Table 1: Demonstration of how parameter synchronization period (K_x) affects final perplexity for two MT-DAO configurations with momentum periods $K_1 = K_v = 16$ for our 16M models. Values show the percentage increase in validation perplexity over the $K_x = 16$ baseline. Higher β leads to **less performance degradation as K_x increases**.

K_x	16	32	64	128	256	512	1024
$\beta_1 = 0.99$	(37.72)	+1.7%	+3.0%	+3.9%	+5.1%	+5.6%	+6.2%
$\beta_1 = 0.995$	(37.65)	+1.0%	+1.6%	+3.2%	+2.8%	+3.4%	+3.7%

Table 1 shows that a MT-DAO configuration with a higher momentum decay β_1 suffers less performance degradation as the parameter synchronization period K_x increases. This improved resilience can be explained by the reduced rate of change in the model parameters, which is quantified in Figure 5. The underlying principle is that the global averaging step is most effective when the worker models have diverged minimally. Let x_t be the synchronized model at the start of a round. After K_x local steps, worker m arrives at state $x_{t+K_x}^m$. Figure 5 shows that high (β_1, ω_1) values reduces the local model change, $\mathbb{E}_m[\|x_{t+K_x}^m - x_t\|_2]$. A smaller per-worker model change bounds the variance across the set of workers ($\{x_{t+K_x}^m\}_{m=1}^M$), mitigating local drift. This enhances convergence robustness because workers compute gradients on models that are closer to the global mean, making their local updates more relevant to the central objective [29].

Slow Momentum as Anchor: Long-term momentum (high β_1 and ω) reduces the rate of change of parameters and optimizer states. This stability ensures worker models diverge less prior to synchronization, **which reduces the performance impact of infrequent synchronization**.

5.3 MT-DAO Outperforms Prior Low-comms Optimizers and Matches DDP (RQ3)

We evaluate MT-DAO on 16M, 125M, and 720M parameter language models against other baselines. We report validation perplexity as a function of both training tokens and wall-clock time. Timings are measured on 4 cloud H100s connected via 50–100 Gbit/s Ethernet, including constant implementation overheads, and accounting for communication–computation overlap in DDP. These measurements are specific to this hardware; Section E provides a bandwidth model that compares communication-efficient methods to DDP across a wider range of interconnects. When reporting time-to-target perplexity, we give improvements in both wall-clock time and training tokens.

Across all scales, MT-DAO consistently improves over ADOPT-DDP and Local ADOPT in both tokens and time, closing the gap to synchronous training and reducing end-to-end wall clock by **6–27%**. At 720M, relative to single-momentum DDP, MT-DAO reaches the same perplexity in **24%** fewer tokens and **35%** less time. Relative to QHADOPT-DDP, MT-DAO trails at 16M, matches at 125M, and at 720M reaches the QHADOPT-DDP target perplexity about **8%** faster in wall-clock and \approx **5%** fewer tokens.

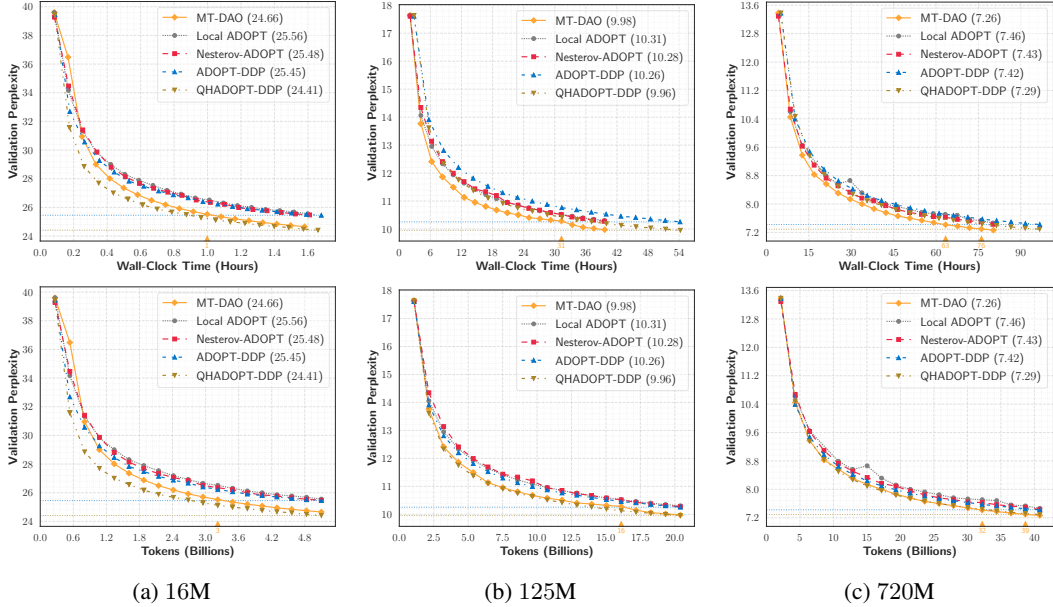


Figure 6: Validation perplexity versus wall-clock time and training tokens for MT-DAO and baselines on models of size (a) 16M, (b) 125M, and (c) 720M models. Horizontal lines denote the two DDP baselines (ADOPT-DDP and QHADOPT-DDP). For each non-DDP method, a colored marker on the x-axis marks the earliest point at which its curve attains a lower/equal perplexity to a DDP variant.

The additional improvements in time are due to MT-DAO communicating $10\times$ less than DDP. The outer Nesterov baseline performs better than Local ADOPT in our setting yet remains below MT-DAO and DDP; matching the findings of Charles et al. [7, Table 4], which reported underperformance relative to DDP by 0.2% to 1.7% at the 550M to 1.3B scale. Mechanistically, Nesterov coalesces per-round gradients and preserves them according to the half-life of the *outer* momentum, whereas MT-DAO implements a finer-grained *inner* multi-timescale modification. We examine how these choices shape worker update trajectories in the next section, however, we do note that MT-DAO ($N = 1$) does not require the additional momentum buffer of Nesterov and has only one additional hyperparameter to tune instead of two.

Improved Performance and Efficiency at Scale: MT-DAO improves performance w.r.t all baselines across model scales, **closing the performance gap to DDP.**

5.4 MT-DAO Aligns Worker Update Trajectories(RQ4)

Having established the performance benefits of MT-DAO, we now investigate the underlying mechanism. We hypothesize that the slow momentum reduces worker drift by keeping the optimization trajectories of individual workers aligned with the global optimization direction. To validate this, we measure the cosine similarity between key optimization vectors. We define the per-round local update as the "pseudo-gradient" ($\Delta^m = x_{t+K}^m - x_t^m$), and the global pseudo-gradient as the average of local ones [43]. To provide a comprehensive comparison, we define the "global momentum" for each method: for MT-DAO and Local ADOPT, it is the average of worker momenta at the end of a round, while for the Nesterov variant, it is the state of the outer Nesterov momentum.

The results in Fig. 7 show that MT-DAO achieves near-perfect alignment (cosine similarity > 0.95) across all four metrics. This indicates that: (1) each worker's update is consistent with its own momentum history (Local PG to Local Mom), (2) workers are in strong agreement with each other (Local PG to Global PG), and (3, 4) both local and global updates are aligned with the long-term global trajectory (Local/Global PG to Global Mom). This demonstrates that the slow momentum acts as a regularizer, ensuring all workers maintain a stable and shared optimization path.

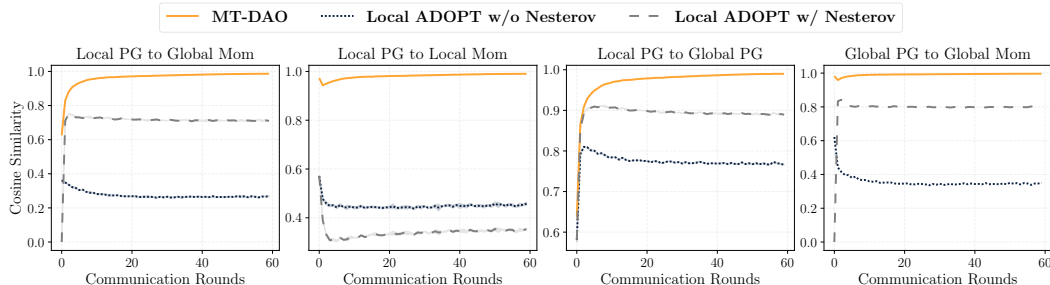


Figure 7: A comparison of update vector alignments for MT-DAO ($\beta_1 = 0.999, \omega_1 = 0.98$) versus Local ADOPT ($\beta_1 = 0.95$), and Local ADOPT ($\beta_1 = 0.95$) with Nesterov. Cosine similarity is measured between: (1) the local pseudo-gradient and global momentum, (2) the local pseudo-gradient and the local momentum, (3) the local and global pseudo-gradients, (4) the local and global momentum. Pseudo-gradient and momentum have been abbreviated as *PG* and *Mom*.

In contrast, the Nesterov outer optimizer presents mixed results. As an EMA of global pseudo-gradients, it is better aligned to the global pseudo-gradient than the Local ADOPT momentum and it improves the alignment between the local and global pseudo-gradients compared to standard Local ADOPT. However, it never reaches the degree of alignment of MT-DAO in any metric.

Slow Momentum as Regularizer: MT-DAO’s slow momentum acts as a regularizer for each worker, ensuring that **local updates remain aligned with their history and the global trajectory**.

6 Related Work

Standard Distributed Data Parallelism’s (DDP) per-step synchronization creates a communication bottleneck [50]. This is mitigated by two orthogonal strategies: payload compression and infrequent synchronization. Compression shrinks transmissions via quantization [2], sparsification [32], mixes thereof [58], low-rank updates [45], or communicating select momentum components [41]. Our work advances infrequent synchronization [51, 39] which allows local updates between communications and is complementary to compression.

Adapting stateful optimizers like Adam to infrequent synchronization is not straightforward. Local Adam [10] provided the first convergence proofs at the cost of synchronizing all optimizer states. Douillard et al. [12], Charles et al. [7] showed that a Nesterov-based outer optimizer improves performance. Recently Jacob et al. [19] improved the communication efficiency of Local Adam by decoupling parameter and momentum sync frequencies. However, these methods use single-timescale optimizers with small β_1 values ill-suited to low communication frequencies due to momentum decay. While naively increasing momentum often harms task performance, recent optimizers that track gradients across multiple timescales have shown significant benefits. QHM [37] decouples momentum decay from gradient weight, while AggMo [36] averages multiple velocity vectors for stability. Building on this, AdEMAMix [40] mixes fast and slow momenta to accelerate convergence, demonstrating that slow momentum acts as memory, reducing forgetting in LLMs. For further related work see Section G.

7 Conclusion

A persistent challenge in distributed training has been the performance gap between fully-synchronous and communication-efficient optimizers. We identify one potential cause for this gap: the rapid decay of momentum in standard optimizers is temporally mismatched with the long intervals inherent to infrequent communication, leading to unstable update directions. We address this with MT-DAO, a multi-timescale optimizer that maintains a stable, long-term (high- β) update direction that persists across communication rounds. Our theory shows that momenta with higher β are less sensitive to synchronization frequency. Furthermore, our experiments on large language models demonstrate that this approach closes the performance gap with DDP and outperforms prior communication-efficient methods. This is achieved by using the slow momentum to maintain a stable, shared optimization

trajectory across workers. These findings establish that managing momentum timescales is a critical factor for performant distributed training, opening new avenues for research into dynamic timescale modulation and integration with compression. Ultimately, this work provides a robust and practical path forward for scaling foundation model training in communication-constrained environments, for cross-datacenter training, or across wide geographic areas.

References

- [1] Kwangjun Ahn, Byron Xu, Natalie Abreu, and John Langford. Dion: Distributed orthonormalized updates. *arXiv preprint arXiv: 2504.05295*, 2025.
- [2] Dan Alistarh, Demjan Grubic, Jerry Li, Ryota Tomioka, and Milan Vojnovic. QSGD: communication-efficient SGD via gradient quantization and encoding. In *Conference on Neural Information Processing Systems (NeurIPS)*, 2017.
- [3] Dan Alistarh, Torsten Hoefler, Mikael Johansson, Nikola Konstantinov, Sarit Khirirat, and Cédric Renggli. The convergence of sparsified gradient methods. In *Conference on Neural Information Processing Systems (NeurIPS)*, 2018.
- [4] Loubna Ben Allal, Anton Lozhkov, Elie Bakouch, Gabriel Martín Blázquez, Guilherme Penedo, Lewis Tunstall, Andrés Marafioti, Hynek Kydlíček, Agustín Piqueres Lajarín, Vaibhav Srivastav, Joshua Lochner, Caleb Fahlgren, Xuan-Son Nguyen, Clémentine Fourrier, Ben Burtenshaw, Hugo Larcher, Haojun Zhao, Cyril Zakka, Mathieu Morlon, Colin Raffel, and Thomas Wolf. Smollm2: When smol goes big - data-centric training of a small language model. *arXiv preprint arXiv:2502.02737*, 2025.
- [5] Yossi Arjevani, Yair Carmon, John C Duchi, Dylan J Foster, Nathan Srebro, and Blake Woodworth. Lower bounds for non-convex stochastic optimization. *Mathematical Programming*, 199(1-2):165–214, 2023.
- [6] Jeremy Bernstein, Jiawei Zhao, Kamyar Azizzadenesheli, and Anima Anandkumar. signsgd with majority vote is communication efficient and fault tolerant. *arXiv preprint arXiv:1810.05291*, 2018.
- [7] Zachary Charles, Gabriel Teston, Lucio Dery, Keith Rush, Nova Fallen, Zachary Garrett, Arthur Szlam, and Arthur Douillard. Communication-efficient language model training scales reliably and robustly: Scaling laws for diloco. *arXiv preprint arXiv:2503.09799*, 2025.
- [8] Xiangning Chen, Chen Liang, Da Huang, Esteban Real, Kaiyuan Wang, Hieu Pham, Xuanyi Dong, Thang Luong, Cho-Jui Hsieh, Yifeng Lu, and Quoc V. Le. Symbolic discovery of optimization algorithms. In *NeurIPS*, 2023.
- [9] Yineng Chen, Zuchao Li, Lefei Zhang, Bo Du, and Hai Zhao. Bidirectional looking with A novel double exponential moving average to adaptive and non-adaptive momentum optimizers. In *ICML, Proceedings of Machine Learning Research*, 2023.
- [10] Ziheng Cheng and Margalit Glasgow. Convergence of distributed adaptive optimization with local updates. In *International Conference on Learning Representations (ICLR)*, 2025.
- [11] Nolan Dey, Bin Claire Zhang, Lorenzo Noci, Mufan Bill Li, Blake Bordelon, Shane Bergsma, Cengiz Pehlevan, Boris Hanin, and Joel Hestness. Don't be lazy: Completep enables compute-efficient deep transformers. *arXiv preprint arXiv: 2505.01618*, 2025.
- [12] Arthur Douillard, Qixuang Feng, Andrei A. Rusu, Rachita Chhaparia, Yani Donchev, Adhiguna Kuncoro, Marc'Aurelio Ranzato, Arthur Szlam, and Jiajun Shen. Diloco: Distributed low-communication training of language models. *arXiv preprint arXiv:2311.08105*, 2023.
- [13] Arthur Douillard, Yanislav Donchev, Keith Rush, Satyen Kale, Zachary Charles, Zachary Garrett, Gabriel Teston, Dave Lacey, Ross McIlroy, Jiajun Shen, Alexandre Ramé, Arthur Szlam, Marc'Aurelio Ranzato, and Paul Barham. Streaming diloco with overlapping communication: Towards a distributed free lunch. *arXiv preprint arXiv:2501.18512*, 2025.

- [14] Alireza Fallah, Aryan Mokhtari, and Asuman Ozdaglar. Personalized federated learning: A meta-learning approach. *arXiv preprint arXiv:2002.07948*, 2020.
- [15] Alexander Hägele, Elie Bakouch, Atli Kosson, Loubna Ben Allal, Leandro von Werra, and Martin Jaggi. Scaling laws and compute-optimal training beyond fixed training durations. In *Conference on Neural Information Processing Systems (NeurIPS)*, 2024.
- [16] Jordan Hoffmann, Sebastian Borgeaud, Arthur Mensch, Elena Buchatskaya, Trevor Cai, Eliza Rutherford, Diego de Las Casas, Lisa Anne Hendricks, Johannes Welbl, Aidan Clark, Tom Hennigan, Eric Noland, Katie Millican, George van den Driessche, Bogdan Damoc, Aurelia Guy, Simon Osindero, Karen Simonyan, Erich Elsen, Jack W. Rae, Oriol Vinyals, and Laurent Sifre. Training compute-optimal large language models. *arXiv preprint arXiv:2203.15556*, 2022.
- [17] Tzu-Ming Harry Hsu, Hang Qi, and Matthew Brown. Measuring the effects of non-identical data distribution for federated visual classification. *arXiv preprint arXiv:1909.06335*, 2019.
- [18] Zhouyuan Huo, Qian Yang, Bin Gu, Lawrence Carin, and Heng Huang. Faster on-device training using new federated momentum algorithm. *arXiv preprint arXiv: 2002.02090*, 2020.
- [19] Alex Iacob, Lorenzo Sani, Mher Safaryan, Paris Giampouras, Samuel Horváth, Andrej Jovanovic, Meghdad Kurmanji, Preslav Aleksandrov, William F. Shen, Xinchu Qiu, and Nicholas D. Lane. Des-loc: Desynced low communication adaptive optimizers for training foundation models. *arXiv preprint arXiv: 2505.22549*, 2025.
- [20] Keller Jordan, Yuchen Jin, Vlado Boza, Jiacheng You, Franz Cesista, Laker Newhouse, and Jeremy Bernstein. Muon: An optimizer for hidden layers in neural networks, 2024. URL <https://kellerjordan.github.io/posts/muon/>.
- [21] Peter Kairouz, H. Brendan McMahan, Brendan Avent, Aurélien Bellet, Mehdi Bennis, Arjun Nitin Bhagoji, Kallista Bonawitz, Zachary Charles, Graham Cormode, Rachel Cummings, Rafael G. L. D’Oliveira, Hubert Eichner, Salim El Rouayheb, David Evans, Josh Gardner, Zachary Garrett, Adrià Gascón, Badih Ghazi, Phillip B. Gibbons, Marco Gruteser, Zaid Harchaoui, Chaoyang He, Lie He, Zhouyuan Huo, Ben Hutchinson, Justin Hsu, Martin Jaggi, Tara Javidi, Gauri Joshi, Mikhail Khodak, Jakub Konečný, Aleksandra Korolova, Farinaz Koushanfar, Sanmi Koyejo, Tancrède Lepoint, Yang Liu, Prateek Mittal, Mehryar Mohri, Richard Nock, Ayfer Özgür, Rasmus Pagh, Mariana Raykova, Hang Qi, Daniel Ramage, Ramesh Raskar, Dawn Song, Weikang Song, Sebastian U. Stich, Ziteng Sun, Ananda Theertha Suresh, Florian Tramèr, Praneeth Vepakomma, Jianyu Wang, Li Xiong, Zheng Xu, Qiang Yang, Felix X. Yu, Han Yu, and Sen Zhao. Advances and open problems in federated learning. *arXiv preprint arXiv:1912.04977*, 2021.
- [22] Satyen Kale, Arthur Douillard, and Yanislav Donchev. Eager updates for overlapped communication and computation in diloco. *arXiv preprint arXiv:2502.12996*, 2025.
- [23] Sai Praneeth Karimireddy, Martin Jaggi, Satyen Kale, Mehryar Mohri, Sashank J Reddi, Sebastian U Stich, and Ananda Theertha Suresh. Mime: Mimicking centralized stochastic algorithms in federated learning. *arXiv preprint arXiv:2008.03606*, 2020.
- [24] Sai Praneeth Karimireddy, Satyen Kale, Mehryar Mohri, Sashank Reddi, Sebastian Stich, and Ananda Theertha Suresh. SCAFFOLD: Stochastic controlled averaging for federated learning. In *International Conference on Machine Learning (ICML)*, 2020.
- [25] Jeonghoon Kim, Byeongchan Lee, Cheonbok Park, Yeontaek Oh, Beomjun Kim, Taehwan Yoo, Seongjin Shin, Dongyoon Han, Jinwoo Shin, and Kang Min Yoo. Peri-In: Revisiting layer normalization in the transformer architecture. *arXiv preprint arXiv: 2502.02732*, 2025.
- [26] Diederik P. Kingma and Jimmy Ba. Adam: A method for stochastic optimization. In *International Conference on Learning Representations (ICLR)*, 2015.
- [27] Jaerin Lee, Bong Gyun Kang, Kihoon Kim, and Kyoung Mu Lee. Grokfast: Accelerated grokking by amplifying slow gradients. *arXiv preprint arXiv: 2405.20233*, 2024.

- [28] Royson Lee, Minyoung Kim, Da Li, Xinchu Qiu, Timothy Hospedales, Ferenc Huszár, and Nicholas Lane. Fed12p: Federated learning to personalize. *Advances in Neural Information Processing Systems*, 36:14818–14836, 2023.
- [29] Tian Li, Anit Kumar Sahu, Manzil Zaheer, Maziar Sanjabi, Ameet Talwalkar, and Virginia Smith. Federated optimization in heterogeneous networks. In *Proceedings of Machine Learning and Systems (MLSys)*, 2020.
- [30] Tian Li, Shengyuan Hu, Ahmad Beirami, and Virginia Smith. Ditto: Fair and robust federated learning through personalization. In *International Conference on Machine Learning (ICML)*, 2021.
- [31] Tao Lin, Sebastian U Stich, Kumar Kshitij Patel, and Martin Jaggi. Don’t use large mini-batches, use local sgd. *arXiv preprint arXiv:1808.07217*, 2018.
- [32] Yujun Lin, Song Han, Huizi Mao, Yu Wang, and Bill Dally. Deep gradient compression: Reducing the communication bandwidth for distributed training. In *International Conference on Learning Representations (ICLR)*, 2018.
- [33] Hong Liu, Zhiyuan Li, David Leo Wright Hall, Percy Liang, and Tengyu Ma. Sophia: A scalable stochastic second-order optimizer for language model pre-training. In *International Conference on Learning Representations (ICLR)*, 2024.
- [34] Yanli Liu, Yuan Gao, and Wotao Yin. An improved analysis of stochastic gradient descent with momentum. *arXiv preprint arXiv:2007.07989*, 2020.
- [35] Ilya Loshchilov and Frank Hutter. Decoupled weight decay regularization. In *International Conference on Learning Representations (ICLR)*, 2019.
- [36] James Lucas, Shengyang Sun, Richard S. Zemel, and Roger B. Grosse. Aggregated momentum: Stability through passive damping. In *International Conference on Learning Representations (ICLR)*, 2019.
- [37] Jerry Ma and Denis Yarats. Quasi-hyperbolic momentum and adam for deep learning. In *International Conference on Learning Representations (ICLR)*, 2019.
- [38] Sam McCandlish, Jared Kaplan, Dario Amodei, and OpenAI Dota Team. An empirical model of large-batch training. *arXiv preprint arXiv: 1812.06162*, 2018.
- [39] Brendan McMahan, Eider Moore, Daniel Ramage, Seth Hampson, and Blaise Aguera y Arcas. Communication-efficient learning of deep networks from decentralized data. In *International Conference on Artificial Intelligence and Statistics (AISTATS)*, 2017.
- [40] Matteo Pagliardini, Pierre Ablin, and David Grangier. The adEMAMix optimizer: Better, faster, older. In *International Conference on Learning Representations (ICLR)*, 2025.
- [41] Bowen Peng, Jeffrey Quesnelle, and Diederik P Kingma. Demo: Decoupled momentum optimization. *arXiv preprint arXiv:2411.19870*, 2024.
- [42] Xinchu Qiu, Javier Fernandez-Marques, Pedro PB Gusmao, Yan Gao, Titouan Parcollet, and Nicholas Donald Lane. Zeroff: Efficient on-device training for federated learning with local sparsity. *arXiv preprint arXiv:2208.02507*, 2022.
- [43] Sashank J. Reddi, Zachary Charles, Manzil Zaheer, Zachary Garrett, Keith Rush, Jakub Konečný, Sanjiv Kumar, and Hugh Brendan McMahan. Adaptive federated optimization. In *International Conference on Learning Representations (ICLR)*, 2021.
- [44] Amirhossein Reisizadeh, Aryan Mokhtari, Hamed Hassani, Ali Jadbabaie, and Ramtin Pedarsani. Fedpaq: A communication-efficient federated learning method with periodic averaging and quantization. In *International Conference on Artificial Intelligence and Statistics (AISTATS)*, 2020.
- [45] Thomas Robert, Mher Safaryan, Ionut-Vlad Modoranu, and Dan Alistarh. Ldadam: Adaptive optimization from low-dimensional gradient statistics. In *International Conference on Learning Representations (ICLR)*, 2025.

- [46] Lorenzo Sani, Alex Jacob, Royson Lee Zeyu Cao, Bill Marino, Yan Gao, Wanru Zhao, Dongqi Cai, Zexi Li, Xinchu Qiu, and Nicholas D. Lane. Photon: Federated llm pre-training. In *Eighth Conference on Machine Learning and Systems*, 2025.
- [47] Felix Sattler, Simon Wiedemann, Klaus-Robert Müller, and Wojciech Samek. Robust and communication-efficient federated learning from non-iid data. *IEEE transactions on neural networks and learning systems*, 2019.
- [48] Bryan Van Scoy, Randy A. Freeman, and Kevin M. Lynch. The fastest known globally convergent first-order method for minimizing strongly convex functions. *IEEE Control. Syst. Lett.*, 2018.
- [49] Andrei Semenov, Matteo Pagliardini, and Martin Jaggi. Benchmarking optimizers for large language model pretraining. *arXiv preprint arXiv: 2509.01440*, 2025.
- [50] Alexander Sergeev and Mike Del Balso. Horovod: fast and easy distributed deep learning in tensorflow. *arXiv preprint arXiv:1802.05799*, 2018.
- [51] Sebastian U. Stich. Local SGD converges fast and communicates little. In *International Conference on Learning Representations (ICLR)*, 2019.
- [52] Jianlin Su, Murtadha H. M. Ahmed, Yu Lu, Shengfeng Pan, Wen Bo, and Yunfeng Liu. Roformer: Enhanced transformer with rotary position embedding. *Neurocomputing*, 2024.
- [53] Ilya Sutskever, James Martens, George E. Dahl, and Geoffrey E. Hinton. On the importance of initialization and momentum in deep learning. In *International Conference on Machine Learning (ICML)*, 2013.
- [54] Shohei Taniguchi, Keno Harada, Gouki Minegishi, Yuta Oshima, Seong Cheol Jeong, Go Nagahara, Tomoshi Iiyama, Masahiro Suzuki, Yusuke Iwasawa, and Yutaka Matsuo. ADOPT: modified adam can converge with any β_2 with the optimal rate. In *Conference on Neural Information Processing Systems (NeurIPS)*, 2024.
- [55] Jianyu Wang, Qinghua Liu, Hao Liang, Gauri Joshi, and H. Vincent Poor. Tackling the Objective Inconsistency Problem in Heterogeneous Federated Optimization. *arXiv preprint arXiv:2007.07481*, 2020.
- [56] Jianyu Wang, Zachary Charles, Zheng Xu, Gauri Joshi, H. Brendan McMahan, Blaise Agueray Arcas, Maruan Al-Shedivat, Galen Andrew, Salman Avestimehr, Katharine Daly, Deepesh Data, Suhas Diggavi, Hubert Eichner, Advait Gadhikar, Zachary Garrett, Antonious M. Girgis, Filip Hanzely, Andrew Hard, Chaoyang He, Samuel Horvath, Zhouyuan Huo, Alex Ingerman, Martin Jaggi, Tara Javidi, Peter Kairouz, Satyen Kale, Sai Praneeth Karimireddy, Jakub Konecny, Sanmi Koyejo, Tian Li, Luyang Liu, Mehryar Mohri, Hang Qi, Sashank J. Reddi, Peter Richtarik, Karan Singhal, Virginia Smith, Mahdi Soltanolkotabi, Weikang Song, Ananda Theertha Suresh, Sebastian U. Stich, Ameet Talwalkar, Hongyi Wang, Blake Woodworth, Shanshan Wu, Felix X. Yu, Honglin Yuan, Manzil Zaheer, Mi Zhang, Tong Zhang, Chunxiang Zheng, Chen Zhu, and Wennan Zhu. A field guide to federated optimization. *arXiv preprint arXiv:2107.06917*, 2021.
- [57] Jue Wang, Yucheng Lu, Binhang Yuan, Beidi Chen, Percy Liang, Christopher De Sa, Christopher Re, and Ce Zhang. Cocktailsgd: Fine-tuning foundation models over 500mbps networks. In *International Conference on Machine Learning (ICML)*, 2023.
- [58] Jue Wang, Yucheng Lu, Binhang Yuan, Beidi Chen, Percy Liang, Christopher De Sa, Christopher Ré, and Ce Zhang. Cocktailsgd: Fine-tuning foundation models over 500mbps networks. In *ICML*, volume 202 of *Proceedings of Machine Learning Research*, pp. 36058–36076. PMLR, 2023.
- [59] Hao Yu, Rong Jin, and Sen Yang. On the linear speedup analysis of communication efficient momentum sgd for distributed non-convex optimization. *arXiv preprint arXiv:1905.03817*, 2019.
- [60] Kun Yuan, Xinmeng Huang, Yiming Chen, Xiaohan Zhang, Yingya Zhang, and Pan Pan. Revisiting optimal convergence rate for smooth and non-convex stochastic decentralized optimization. *arXiv preprint arXiv:2210.07863*, 2022.

- [61] Hanlin Zhang, Depen Morwani, Nikhil Vyas, Jingfeng Wu, Difan Zou, Udaya Ghai, Dean Foster, and Sham M. Kakade. How does critical batch size scale in pre-training? In *International Conference on Learning Representations (ICLR)*, 2025.

Appendix

Table of Contents

A	Limitations	16
B	Experimental Details	16
B.1	Architecture Details and Parametrization	16
B.2	Optimizer Hyperparameter Sweeping Procedure	16
B.3	Optimizer Tuning Results	17
C	Deterministic Optimizer-specific Variants of MT-DAO	18
	MT-DAO-ADOPT	18
	MT-DAO-SGDM	18
D	Convergence Analysis of MT-DAO-SGDM	20
D.1	Key Lemmas	24
E	Wall-Clock Time Modeling	28
E.1	Wall-Clock Time Model	28
E.2	Experimental Configuration	29
E.3	Modeling Results	29
F	Derivations of Mutual Information and Variance	30
F.1	Variance of Local Momentum	30
F.2	Mutual Information	31
G	Extended Related Work	32
H	Additional Results	33
I	LLM Usage Declaration	33

A Limitations

Limitations. First, our empirical validation is limited to models up to 720M parameters. Second, our experiments use ADOPT instead of Adam, this avoids the need to tune the β_2 of the second momentum, simplifying experimental design. Third, we preferred a detailed investigation of the training dynamics of the highly memory and communication-efficient MT-DAO ($N = 1$) over increasing the number of momenta, which brings diminishing returns [36, 37].

B Experimental Details

Here we provide additional experimental details complementing those in Section 4.1, including: a) model architecture details and the model parameterization (Section B.1), b) our hyperparameter sweep procedure to select optimizer-specific settings (Section B.2), and c) the results of our tuning sweeps for MT-DAO.

B.1 Architecture Details and Parametrization

Table 2: Model architecture and training hyperparameters. Architectural parameters include the number of transformer blocks (#Blocks), attention heads (#Heads), embedding dimension (d_{model}), vocabulary size ($|\mathcal{V}|$), and feedforward expansion ratio (Exp. Ratio). Key training parameters are the global batch size ($|\mathcal{B}_G|$) and the total number of training steps (T). All models use RoPE positional embeddings [52], the SiLU activation function, norm-based gradient clipping with a bound of ρ , and are initialized with a typical [49, 11] $\sigma = 0.02$. Sequence length is standard for models at these scales.

Model Size	Blocks	d_{model}	$ \mathcal{V} $	#Heads	Exp.~Ratio	ROPE θ	ACT	Init σ	ρ	Seq Len	$ \mathcal{B}_G $	T
16M	4	256	50K	4	4	10000	SiLU	0.02	1.0	2048	64	4608, 38912
125M	12	768	50K	12	4	10000	SiLU	0.02	1.0	2048	256	38912
720M	12	2048	50K	16	4	10000	SiLU	0.02	1.0	2048	512	38912

Table 2 summarizes the architectural details of our models, which follow established practices for large language models at their respective scales. To improve training stability and final performance, we adopt two key modifications. First, following the recommendations of Kim et al. [25], we use a Peri-LayerNorm transformer structure instead of pre-norm. Second, we use the CompleteP [11] parametrization with $\alpha = 1.0$, which enables the effective transfer of optimizer hyperparameters from a small model to its larger-scale counterparts in a one-shot manner. This property allows us to perform comprehensive hyperparameter sweeps on our smallest model size and reserve computationally expensive scaling experiments for direct comparisons against baselines.

We set batch sizes and training durations following recent best practices [61]. For the smallest model size, the initial batch size is determined using the noise-scale estimator for the critical batch size [38] and then doubled until the efficiency deviates from a linear trend by 20%. For our 125M and 720M models we follow the batch size recommendations from Semenov et al. [49]. Training durations are set as multiples of the compute-optimal token budget [16]: for the 16M model, we tune using $\approx 2\times$ this budget and run baseline comparisons at $\approx 16\times$; for the 125M model, we use $\approx 8\times$; and for the 720M model, we use $\approx 2.83\times$. We chose the 720M model size as a good balance between scale and computational efficiency following Semenov et al. [49].

All models are trained using the warmup-stable-decay (WSD) learning rate schedule [15], with warmup and decay periods selected based on established recommendations [61, 15, 4, 49]. For the 16M model tuning runs, which last 4608 steps, the warmup period is set to $T_{\text{WARM}} = 512$ steps. For all longer training runs and baseline comparisons, we use the industry-standard warmup of $T_{\text{WARM}} = 2048$ steps. We use a cooldown period equal to the warmup period in all cases, using 1-sqrt cooldown [15].

B.2 Optimizer Hyperparameter Sweeping Procedure

Our tuning procedure is designed to ensure that both our method and the baselines are evaluated under their optimal DDP configurations, providing a fair comparison. Given that previous work has shown

that the learning rate (LR) tends to transfer effectively between DDP and distributed settings [19], we first tune all parameters to achieve the best possible performance under DDP and then transfer these settings to MT-DAO. Unlike methods such as AdEMAMix that use schedulers for optimizer parameters, we employ a simple switch from a base optimizer (e.g., ADOPT) to its multi-timescale variant at the end of the warmup period. This necessitates a two-phase LR tuning process to ensure identical starting conditions for both optimizers:

1. **Phase 1: Base Optimizer Tuning.** We first tune the learning rate for the base optimizer over the entire training run to achieve the lowest final perplexity. This ensures the baseline itself is as strong as possible.
2. **Phase 2: MT-DAO/Quasi-hyperbolic Tuning.** Using the model state from the end of the base optimizer’s warmup, we then tune the learning rate for the post-switch phase of MT-DAO and of its DDP analogue. With a WSD scheduler, this corresponds to tuning the LR for the constant "stable" portion of training and for the cooldown.

While more complex scheduling manipulations might yield further gains for MT-DAO, this two-phase approach provides the cleanest methodology for comparison. For every combination of momentum decay rates (β 's) and convex coefficients (ω 's) used by MT-DAO, we independently perform this tuning procedure. For ADOPT the LR sweeps in both phases search over values between 2^{-10} and 2^{-6} using powers of two, with the search grid refined by manually adding half-power steps (e.g., $2^{-8.5}$, $2^{-7.5}$, $2^{-6.5}$) around the optimal value.

B.3 Optimizer Tuning Results

First, our tuning of ADOPT for DDP revealed an optimal lr $\eta^* = 2^{-8}$. We now present the results of our tuning for the post-warmup lr for MT-DAO-ADOPT with $N = 1$ first momenta in Fig. 8.

A clear trend emerges from our results: methods with higher momentum decay rates (β s) or higher weights (ω s) ascribed to the slow-moving momenta can tolerate significantly higher learning rates than standard momentum methods. This finding is in strong agreement with the previous findings of Lucas et al. [36], who similarly found that AggMo can effectively utilize learning rates that are orders of magnitude higher than those suitable for classical momentum.

Takeaway: Multi-timescale optimizers that emphasize slow-moving momenta (via high β or ω values) are not only more stable but can also leverage much higher learning rates, enabling faster convergence than their single-timescale counterparts.

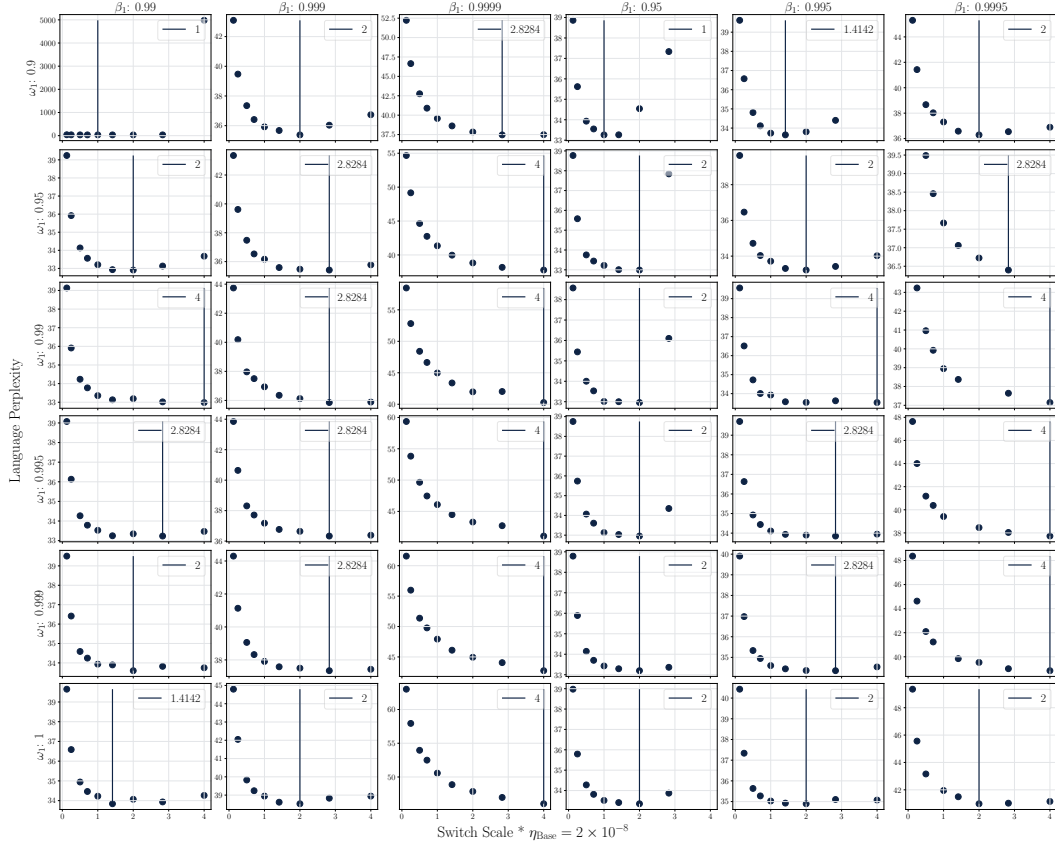


Figure 8: Visualizing the learning rate sweeps for different MT-DAO configurations. Each subplot shows the final perplexity for a given convex coefficient (ω) and momentum decay (β_1), where $\beta_2 = 0.999$ was kept constant. The sweep demonstrates that the optimal learning rate and final performance are highly dependent on the choice of these internal hyperparameters, with $\beta_1 \in [0.995, 0.999]$ and $\omega \in [0.9, 0.99]$ performing best for these short tuning experiments. The vertical line in each subplot marks the best-performing lr for that configuration. Switch scale refers to the multiple of the base learning rate that we select, the chosen learning rate can be computed via multiplication with η_{BASE} .

C Deterministic Optimizer-specific Variants of MT-DAO

Algorithm 2 MT-DAO-ADOPT

Require: Model tensors, hyper-parameters

- 1: $x_0 \in \mathbb{R}^d, \{\bar{u}_{-1}^j\}_{j=1}^N \in (\mathbb{R}^d)^N, \bar{v}_{-1} \in \mathbb{R}^d$ — initial params, N first momenta, second momentum
- 2: $\{\beta_{1,j}\}_{j=1}^N, \beta_2 \in [0, 1)$ — decay rates for each momentum state
- 3: $\{\omega_j\}_{j=1}^N \in [0, 1]$ — convex combination coefficients for first momenta, $\sum_{j=1}^N \omega_j \leq 1.0$
- 4: $\{c_t\}_{t=0}^{T-1}, \{\eta_t\}_{t=0}^{T-1}$ — clipping and learning-rate schedules
- 5: $T, M \in \mathbb{N}_+$ — total optimization steps and number of workers
- 6: $K_x, \{K_j\}_{j=1}^N, K_v \in (\mathbb{N}_+)^{N+2}$ — communication periods for parameters and states
- 7: **OuterOpt** : $\mathbb{R}^d \rightarrow \mathbb{R}^d$ — update params using an outer optimizer, averaging by default

Ensure: $x_T, \{u_{T-1}^j\}_{j=1}^N, v_{T-1}$

- 8: **for each worker** m : initialize $x_0^m, \{u_{-1}^{j,m}\}, v_{-1}^m$
 - 9: **for** $t = 0, \dots, T - 1$ **do**
 - 10: **for all workers** $m = 0, \dots, M - 1$ **in parallel do**
 - 11: $g_t^m \leftarrow \nabla F(x_t^m; \xi_t^m)$ stochastic gradient
 - 12: $v_t^m \leftarrow \beta_2 \bar{v}_{t-1} + (1 - \beta_2)(g_t^m)^2$ update second momentum with raw gradient
 - 13: $\bar{v}_t \leftarrow$ **if** $(t \bmod K_v = 0)$ **then** $\mathbb{E}_m[v_t^m]$ **else** v_t^m sync v every K_v steps
 - 14: $\hat{g}_t^m \leftarrow \frac{g_t^m}{\sqrt{v_t^m + \epsilon}}$ normalize gradient (ADOPT core step)
 - 15: $\tilde{g}_t^m \leftarrow$ **clip** (\hat{g}_t^m, c_t) clip the normalized gradient
 - 16: **for** $j = 1$ **to** N **do** update N first momenta
 - 17: $u_t^{j,m} \leftarrow \beta_{1,j} \bar{u}_{t-1}^j + (1 - \beta_{1,j}) \tilde{g}_t^m$ use clipped, normalized gradient
 - 18: $\bar{u}_t^j \leftarrow$ **if** $(t \bmod K_j = 0)$ **then** $\mathbb{E}_m[u_t^{j,m}]$ **else** $u_t^{j,m}$ sync u^j every K_j steps
 - 19: $\Delta_t^m \leftarrow (1 - \sum_{j=1}^N \omega_j) \tilde{g}_t^m + \sum_{j=1}^N \omega_j u_t^{j,m}$ form combined update direction
 - 20: $x_{t+1}^m \leftarrow \bar{x}_t - \eta_t \Delta_t^m$ apply combined update
 - 21: $\bar{x}_{t+1} \leftarrow$ **if** $((t + 1) \bmod K_x = 0)$ **then** **OuterOpt** $(\mathbb{E}_m[x_{t+1}^m])$ **else** x_{t+1}^m sync x every K_x steps
-

Algorithm 3 MT-DAO-SGDM

Require: Model tensors, hyper-parameters

- 1: $x_0 \in \mathbb{R}^d, \{\bar{u}_{-1}^j\}_{j=1}^N \in (\mathbb{R}^d)^N$ — initial params, N first momenta
- 2: $\{\beta_{1,j}\}_{j=1}^N \in [0, 1)$ — decay rates for each momentum state
- 3: $\{\omega_j\}_{j=1}^N \in [0, 1]$ — convex combination coefficients for first momenta, $\sum_{j=1}^N \omega_j \leq 1.0$
- 4: $\rho \in \mathbb{R}_+, \{\eta_t\}_{t=0}^{T-1}$ — clipping radius, learning-rate schedule
- 5: $T, M \in \mathbb{N}_+$ — total optimization steps and number of workers
- 6: $K_x, \{K_j\}_{j=1}^N \in (\mathbb{N}_+)^{N+1}$ — communication periods for parameters and states
- 7: **OuterOpt** : $\mathbb{R}^d \rightarrow \mathbb{R}^d$ — update params using an outer optimizer, averaging by default

Ensure: $x_T, \{u_{T-1}^j\}_{j=1}^N$

- 8: **for each worker** m : initialize $x_0^m, \{u_{-1}^{j,m}\}$
 - 9: **for** $t = 0, \dots, T - 1$ **do**
 - 10: **for all workers** $m = 0, \dots, M - 1$ **in parallel do**
 - 11: $\hat{g}_t^m \leftarrow$ **clip** $(\nabla F(x_t^m; \xi_t^m), \rho)$ clipped stochastic gradient
 - 12: **for** $j = 1$ **to** N **do** update N first momenta
 - 13: $u_t^{j,m} \leftarrow \beta_{1,j} \bar{u}_{t-1}^j + (1 - \beta_{1,j}) \hat{g}_t^m$
 - 14: $\bar{u}_t^j \leftarrow$ **if** $(t \bmod K_j = 0)$ **then** $\mathbb{E}_m[u_t^{j,m}]$ **else** $u_t^{j,m}$ sync u^j every K_j steps
 - 15: $\Delta_t^m \leftarrow (1 - \sum_{j=1}^N \omega_j) \hat{g}_t^m + \sum_{j=1}^N \omega_j u_t^{j,m}$ form combined update direction (unnormalized)
 - 16: $x_{t+1}^m \leftarrow \bar{x}_t - \eta_t \Delta_t^m$
 - 17: $\bar{x}_{t+1} \leftarrow$ **if** $((t + 1) \bmod K_x = 0)$ **then** **OuterOpt** $(\mathbb{E}_m[x_{t+1}^m])$ **else** x_{t+1}^m sync x every K_x steps
-

D Convergence Analysis of MT-DAO-SGDM

Algorithm 4 MT-DAO-SGDM, probabilistic variant

Require: Model tensors, hyper-parameters

- 1: $x_0 \in \mathbb{R}^d, \{u_{-1}^j\}_{j=1}^N \in (\mathbb{R}^d)^N$ — initial parameters, N first momenta
- 2: $\{\beta_j\}_{j=1}^N \in [0, 1]$ — decay rates for each momentum state
- 3: $\{\omega_j\}_{j=1}^N \in [0, 1]$ — convex combination of non-negative coefficients for first momenta, $\sum_{j=1}^N \omega_j = 1$
- 4: $\{\eta_t\}_{t=0}^{T-1}$ — learning-rate schedule
- 5: $T, M \in \mathbb{N}_+$ — total optimization steps and number of workers
- 6: $p_x = \frac{1}{K_x}, \{p_j = \frac{1}{K_j}\}_{j=1}^N \in [0, 1]^{N+1}$ — communication periods/probabilities for parameters and states

Ensure: $x_T, \{u_{T-1}^j\}_{j=1}^N$

- 7: **for each worker** m : initialize $x_0^m, \{u_{-1}^{j,m}\}$
 - 8: **for** $t = 0, \dots, T - 1$ **do**
 - 9: **for all workers** $m = 0, \dots, M - 1$ **in parallel do**
 - 10: $g_t^m \leftarrow \nabla F_m(x_t^m; \xi_t^m)$ stochastic gradient
 - 11: **for** $j = 1$ **to** N **do** update N first momenta
 - 12: $u_t^{j,m} \leftarrow \begin{cases} \mathbb{E}_m[\beta_j u_{t-1}^{j,m} + (1 - \beta_j)g_t^m], & \text{with probability } p_j \\ \beta_j u_{t-1}^{j,m} + (1 - \beta_j)g_t^m, & \text{with probability } 1 - p_j \end{cases}$ sync u
 - 13: $\Delta_t^m \leftarrow \sum_{j=1}^N \omega_j u_t^{j,m}$ form combined update direction
 - 14: $x_{t+1}^m \leftarrow \begin{cases} \mathbb{E}_m[x_t^m - \eta_t \Delta_t^m], & \text{with probability } p_x \\ x_t^m - \eta_t \Delta_t^m, & \text{with probability } 1 - p_x \end{cases}$ sync x
-

In order to facilitate the technical presentation, we model synchronization frequencies by assigning probabilities to each averaging event. For example, the parameters x_t^m are synchronized with the probability $p_x = \frac{1}{K_x}$, which is statistically equivalent to performing the averaging in every $\frac{1}{p_x} = K_x$ iteration. Similarly, momentum $u_t^{j,m}$ synchronization happens with probability $p_j = \frac{1}{K_j}$, which can differ from p_x . Note that QHM structure is included since we can choose $\beta_1 = 0$ and get $u_t^{1,m} = g_t^m$.

Auxiliary notation. Let \mathbb{E}_m and \mathbb{E}_j be the averaging operators with weights $\frac{1}{M}$ across M workers and ω_j across N momenta.

$$\begin{aligned}
 u_t^j &\stackrel{\text{def}}{=} \mathbb{E}_m[u_t^{j,m}] = \beta_j u_{t-1}^j + (1 - \beta_j)g_t, \text{ where } g_t = \mathbb{E}_m[g_t^m] \\
 x_{t+1}^{j,m} &\stackrel{\text{def}}{=} \begin{cases} \mathbb{E}_m[x_t^{j,m} - \eta u_t^{j,m}], & \text{with probability } p_x \\ x_t^{j,m} - \eta u_t^{j,m}, & \text{with probability } 1 - p_x \end{cases} \\
 x_{t+1}^j &\stackrel{\text{def}}{=} \mathbb{E}_m[x_{t+1}^{j,m}] = x_t^j - \eta u_t^j, \quad x_{t+1}^m = \mathbb{E}_j[x_{t+1}^{j,m}] = (\text{line 14}).
 \end{aligned}$$

For the sake of notation, we also let $u_t^m = \Delta_t^m = \mathbb{E}_j[u_t^{j,m}]$, $u_t = \mathbb{E}_m[u_t^m]$, $x_t = \mathbb{E}_m[x_t^m]$ in the upcoming derivations.

Step 1 (virtual iterates). Letting $x_{-1}^j = x_0^j = x_0$, define the global virtual iterations as follows

$$z_t^j \stackrel{\text{def}}{=} \frac{1}{1 - \beta_j} x_t^j - \frac{\beta_j}{1 - \beta_j} x_{t-1}^j, \quad \text{and} \quad z_t \stackrel{\text{def}}{=} \mathbb{E}_j[z_t^j] \quad \text{for } t \geq 0.$$

The key property of this virtual iterates we are going to exploit in the next steps is that they follow averaged gradients, namely for any $t \geq 0$ we have

$$\begin{aligned}
z_{t+1} - z_t &= \mathbb{E}_j[z_{t+1}^j - z_t^j] \\
&= \mathbb{E}_j \left[\left(\frac{1}{1-\beta_j} x_{t+1}^j - \frac{\beta_j}{1-\beta_j} x_t^j \right) - \left(\frac{1}{1-\beta_j} x_t^j - \frac{\beta_j}{1-\beta_j} x_{t-1}^j \right) \right] \\
&= \mathbb{E}_j \left[\frac{1}{1-\beta_j} (x_{t+1}^j - x_t^j) - \frac{\beta_j}{1-\beta_j} (x_t^j - x_{t-1}^j) \right] \\
&= \mathbb{E}_j \left[\frac{1}{1-\beta_j} (-\eta u_t^j) - \frac{\beta_j}{1-\beta_j} (-\eta u_{t-1}^j) \right] \\
&= \mathbb{E}_j \left[\frac{-\eta}{1-\beta_j} (u_t^j - \beta_j u_{t-1}^j) \right] = \mathbb{E}_j[-\eta g_t] = -\eta g_t.
\end{aligned}$$

Step 2 (smoothness over virtual iterates). Then we apply smoothness of the global loss function f over these global virtual iterates.

$$\begin{aligned}
f(z_{t+1}) &\leq f(z_t) + \langle \nabla f(z_t), z_{t+1} - z_t \rangle + \frac{L}{2} \|z_{t+1} - z_t\|^2 \\
&= f(z_t) + \underbrace{\langle \nabla f(x_t), z_{t+1} - z_t \rangle}_I + \underbrace{\langle \nabla f(z_t) - \nabla f(x_t), z_{t+1} - z_t \rangle}_{II} + \underbrace{\frac{L}{2} \|z_{t+1} - z_t\|^2}_{III}.
\end{aligned}$$

In the next step, we separately bound each term appearing in the above bound.

Step 3a (one step progress). Bounding term I.

$$\begin{aligned}
&\mathbb{E} \langle \nabla f(x_t), z_{t+1} - z_t \rangle \\
&= -\eta \mathbb{E} \left\langle \nabla f(x_t), \frac{1}{M} \sum_{m=1}^M g_t^m \right\rangle = -\eta \mathbb{E} \left\langle \nabla f(x_t), \frac{1}{M} \sum_{m=1}^M \nabla f_m(x_t^m) \right\rangle \\
&= -\frac{\eta}{2} \mathbb{E} \|\nabla f(x_t)\|^2 - \frac{\eta}{2} \mathbb{E} \left\| \frac{1}{M} \sum_{m=1}^M \nabla f_m(x_t^m) \right\|^2 + \frac{\eta}{2} \mathbb{E} \left\| \nabla f(x_t) - \frac{1}{M} \sum_{m=1}^M \nabla f_m(x_t^m) \right\|^2 \\
&= -\frac{\eta}{2} \mathbb{E} \|\nabla f(x_t)\|^2 - \frac{\eta}{2} \mathbb{E} \left\| \frac{1}{M} \sum_{m=1}^M \nabla f_m(x_t^m) \right\|^2 + \frac{\eta}{2} \mathbb{E} \left\| \frac{1}{M} \sum_{m=1}^M \nabla f_m(x_t) - \nabla f_m(x_t^m) \right\|^2 \\
&\leq -\frac{\eta}{2} \mathbb{E} \|\nabla f(x_t)\|^2 - \frac{\eta}{2} \mathbb{E} \left\| \frac{1}{M} \sum_{m=1}^M \nabla f_m(x_t^m) \right\|^2 + \frac{\eta}{2M} \sum_{m=1}^M \mathbb{E} \|\nabla f_m(x_t) - \nabla f_m(x_t^m)\|^2 \\
&\leq -\frac{\eta}{2} \mathbb{E} \|\nabla f(x_t)\|^2 - \frac{\eta}{2} \mathbb{E} \left\| \frac{1}{M} \sum_{m=1}^M \nabla f_m(x_t^m) \right\|^2 + \frac{\eta L^2}{2M} \sum_{m=1}^M \underbrace{\mathbb{E} \|x_t - x_t^m\|^2}_{\text{Lemma 3}}.
\end{aligned}$$

Step 3b (one step progress). Bounding term II.

$$\begin{aligned}
\mathbb{E} \langle \nabla f(z_t) - \nabla f(x_t), z_{t+1} - z_t \rangle &= -\eta \mathbb{E} \left\langle \nabla f(z_t) - \nabla f(x_t), \frac{1}{M} \sum_{m=1}^M \nabla f_m(x_t^m) \right\rangle \\
&\leq \frac{\eta \rho}{2} \mathbb{E} \|\nabla f(z_t) - \nabla f(x_t)\|^2 + \frac{\eta}{2\rho} \mathbb{E} \left\| \frac{1}{M} \sum_{m=1}^M \nabla f_m(x_t^m) \right\|^2 \\
&\leq \frac{\eta \rho L^2}{2} \underbrace{\mathbb{E} \|z_t - x_t\|^2}_{\text{Lemma 2}} + \frac{\eta}{2\rho} \mathbb{E} \left\| \frac{1}{M} \sum_{m=1}^M \nabla f_m(x_t^m) \right\|^2.
\end{aligned}$$

Step 3c (one step progress). Bounding term III.

$$\begin{aligned}
\frac{L}{2}\mathbb{E}\|z_{t+1} - z_t\|^2 &= \frac{\eta^2 L}{2}\mathbb{E}\left\|\frac{1}{M}\sum_{m=1}^M g_t^m\right\|^2 \\
&= \frac{\eta^2 L}{2}\mathbb{E}\left\|\frac{1}{M}\sum_{m=1}^M g_t^m - \nabla f_m(x_t^m)\right\|^2 + \frac{\eta^2 L}{2}\mathbb{E}\left\|\frac{1}{M}\sum_{m=1}^M \nabla f_m(x_t^m)\right\|^2 \\
&= \frac{\eta^2 L}{2M^2}\sum_{m=1}^M \mathbb{E}\|g_t^m - \nabla f_m(x_t^m)\|^2 + \frac{\eta^2 L}{2}\mathbb{E}\left\|\frac{1}{M}\sum_{m=1}^M \nabla f_m(x_t^m)\right\|^2 \\
&\leq \frac{\eta^2 L}{2M}\sigma^2 + \frac{\eta^2 L}{2}\mathbb{E}\left\|\frac{1}{M}\sum_{m=1}^M \nabla f_m(x_t^m)\right\|^2.
\end{aligned}$$

Step 3abc (one step progress). Combining previous bounds.

$$\begin{aligned}
\mathbb{E}f(z_{t+1}) - \mathbb{E}f(z_t) &\leq \underbrace{\mathbb{E}\langle \nabla f(x_t), z_{t+1} - z_t \rangle}_I + \underbrace{\mathbb{E}\langle \nabla f(z_t) - \nabla f(x_t), z_{t+1} - z_t \rangle}_{II} + \underbrace{\mathbb{E}\frac{L}{2}\|z_{t+1} - z_t\|^2}_{III} \\
&\leq -\frac{\eta}{2}\mathbb{E}\|\nabla f(x_t)\|^2 - \frac{\eta}{2}\mathbb{E}\left\|\frac{1}{M}\sum_{m=1}^M \nabla f_m(x_t^m)\right\|^2 + \frac{\eta L^2}{2M}\sum_{m=1}^M \underbrace{\mathbb{E}\|x_t - x_t^m\|^2}_{\text{Lemma 3}} \\
&\quad + \frac{\eta\rho L^2}{2}\underbrace{\mathbb{E}\|z_t - x_t\|^2}_{\text{Lemma 2}} + \frac{\eta}{2\rho}\mathbb{E}\left\|\frac{1}{M}\sum_{m=1}^M \nabla f_m(x_t^m)\right\|^2 \\
&\quad + \frac{\eta^2 L}{2K}\sigma^2 + \frac{\eta^2 L}{2}\mathbb{E}\left\|\frac{1}{M}\sum_{m=1}^M \nabla f_m(x_t^m)\right\|^2 \\
&\leq -\frac{\eta}{2}\mathbb{E}\|\nabla f(x_t)\|^2 - \frac{\eta}{2}\left(1 - \frac{1}{\rho} - \eta L\right)\mathbb{E}\left\|\frac{1}{M}\sum_{m=1}^M \nabla f_m(x_t^m)\right\|^2 \\
&\quad + \frac{\eta\rho L^2}{2}\underbrace{\mathbb{E}\|z_t - x_t\|^2}_{\text{Lemma 2}} + \frac{\eta L^2}{2M}\sum_{m=1}^M \underbrace{\mathbb{E}\|x_t - x_t^m\|^2}_{\text{Lemma 3}} + \frac{\eta^2 L}{2M}\sigma^2.
\end{aligned}$$

Step 4 (final). Now we average over the iterates and apply the bounds derived in Lemmas 2 and 3.

$$\begin{aligned}
\frac{\mathbb{E}[f(z_T) - f(z_0)]}{T} &= \frac{1}{T} \sum_{t=0}^{T-1} \mathbb{E}[f(z_{t+1}) - f(z_t)] \\
&\leq -\frac{\eta}{2T} \sum_{t=0}^{T-1} \mathbb{E} \|\nabla f(x_t)\|^2 - \frac{\eta}{2} \left(1 - \frac{1}{\rho} - \eta L\right) \frac{1}{T} \sum_{t=0}^{T-1} \mathbb{E} \left\| \frac{1}{M} \sum_{m=1}^M \nabla f_m(x_t^m) \right\|^2 \\
&\quad + \underbrace{\frac{\eta \rho L^2}{2} \frac{1}{T} \sum_{t=0}^{T-1} \mathbb{E} \|z_t - x_t\|^2}_{\text{Lemma 1}} + \underbrace{\frac{\eta L^2}{2} \frac{1}{TM} \sum_{t=0}^{T-1} \sum_{m=1}^M \mathbb{E} \|x_t - x_t^m\|^2 + \frac{\eta^2 L}{2M} \sigma^2}_{\text{Lemma 2}} \\
&\leq -\frac{\eta}{2T} \sum_{t=0}^{T-1} \mathbb{E} \|\nabla f(x_t)\|^2 - \frac{\eta}{2} \left(1 - \frac{1}{\rho} - \eta L\right) \frac{1}{T} \sum_{t=0}^{T-1} \mathbb{E} \left\| \frac{1}{M} \sum_{m=1}^M \nabla f_m(x_t^m) \right\|^2 + \frac{\eta^2 L}{2M} \sigma^2 \\
&\quad + \frac{\eta \rho L^2}{2} \left(\frac{\eta^2 \beta_\omega^2}{M} \sigma^2 + \eta^2 \beta_\omega^2 \frac{1}{T} \sum_{\tau=0}^{T-1} \mathbb{E} \left\| \frac{1}{M} \sum_{m=1}^M \nabla f_m(x_\tau^m) \right\|^2 \right) \\
&\quad + \frac{\eta L^2}{2} \left(12\eta^2 (B^2 - 1)\psi \cdot \frac{1}{T} \sum_{t=0}^{T-1} \mathbb{E} \|\nabla f(\theta^t)\|^2 + 4\eta^2 \psi (\sigma^2 + 3G^2) \right) \\
&\leq -\frac{\eta}{2} (1 - 12\eta^2 L^2 (B^2 - 1)\psi) \frac{1}{T} \sum_{t=0}^{T-1} \mathbb{E} \|\nabla f(x_t)\|^2 \\
&\quad - \frac{\eta}{2} \left(1 - \frac{1}{\rho} - \eta L - \eta^2 \beta_\omega^2 \rho L^2\right) \frac{1}{T} \sum_{t=0}^{T-1} \mathbb{E} \left\| \frac{1}{M} \sum_{m=1}^M \nabla f_m(x_t^m) \right\|^2 \\
&\quad + \frac{\eta^2 L}{2M} \sigma^2 + \frac{\eta^3 \rho L^2 \beta_\omega^2}{2M} \sigma^2 + 2\eta^3 L^2 \psi (\sigma^2 + 3G^2).
\end{aligned}$$

Next, we choose $\rho = 2$ and step size η such that

$$\begin{aligned}
12\eta^2 L^2 (B^2 - 1)\psi &\leq \frac{1}{2} \iff \text{to bound the first term} \\
\eta L + 2\eta^2 \beta_\omega^2 L^2 &\leq \frac{1}{2} \iff \text{to bound the second term} \\
12\eta^2 L^2 \psi &\leq \frac{1}{2} \iff \text{from Lemma 3}
\end{aligned}$$

Notice that

$$\eta_0 \stackrel{\text{def}}{=} \left(4L \max \left(\beta_\omega, 6\sqrt{\psi \max(1, B^2 - 1)} \right) \right)^{-1}$$

satisfies all three bounds. Then, with any $\eta \leq \eta_0$ we get

$$\begin{aligned}
\frac{\mathbb{E}[f(z_T) - f(z_0)]}{T} &\leq -\frac{\eta}{4T} \sum_{t=0}^{T-1} \mathbb{E} \|\nabla f(x_t)\|^2 \\
&\quad + \frac{\eta^2 L}{2M} \sigma^2 + \frac{\eta^3 \rho L^2 \beta_\omega^2}{2M} \sigma^2 + 2\eta^3 L^2 \psi (\sigma^2 + 3G^2).
\end{aligned}$$

Noticing that $z_0 = x_0$ and $f^* \leq f(z_T)$, we have

$$\frac{1}{T} \sum_{t=0}^{T-1} \mathbb{E} \|\nabla f(x_t)\|^2 \leq \frac{4(f(x_0) - f^*)}{\eta T} + \frac{2\eta L}{M} \sigma^2 + \frac{4\eta^2 L^2 \beta_\omega^2}{M} \sigma^2 + 8\eta^2 L^2 \psi (\sigma^2 + 3G^2).$$

Furthermore, choosing $\eta = \min(\eta_0, \frac{1}{\sqrt{T}})$, we get the following rate:

$$\begin{aligned}
& \frac{1}{T} \sum_{t=0}^{T-1} \mathbb{E} \|\nabla f(x_t)\|^2 \\
& \leq \max\left(1, \frac{1}{\eta_0 \sqrt{T}}\right) \frac{4(f(x_0) - f^*)}{\sqrt{T}} + \frac{2L\sigma^2}{M\sqrt{T}} + \frac{4L^2\beta_\omega^2\sigma^2}{MT} + \frac{8L^2\psi(\sigma^2 + 3G^2)}{T} \\
& \leq \frac{4(f(x_0) - f^*)}{\sqrt{T}} + \frac{2L\sigma^2}{M\sqrt{T}} + \frac{4(f(x_0) - f^*)}{\eta_0 T} + \frac{4L^2\beta_\omega^2\sigma^2}{MT} + \frac{8L^2\psi(\sigma^2 + 3G^2)}{T} \\
& = \frac{4}{\sqrt{T}} \left(f(x_0) - f^* + \frac{L\sigma^2}{2M} \right) + \mathcal{O}\left(\frac{1 + \beta_\omega^2 + \psi}{T}\right).
\end{aligned}$$

D.1 Key Lemmas

Lemma 2. For all $T \geq 1$, we have

$$\sum_{t=0}^{T-1} \|z_t - x_t\|^2 \leq \frac{\eta^2 \beta_\omega^2}{M} T \sigma^2 + \eta^2 \beta_\omega^2 \sum_{t=0}^{T-1} \mathbb{E} \left\| \frac{1}{M} \sum_{m=1}^M \nabla f_m(x_t^m) \right\|^2, \quad (3)$$

where

$$\beta_\omega \stackrel{\text{def}}{=} \sum_{j=1}^N \frac{\omega_j \beta_j}{1 - \beta_j}.$$

Proof. Since $u_{-1} = 0$, unrolling the update rule of momentum, for any $t \geq 0$ we get

$$u_t^j = \beta_j u_{t-1}^j + (1 - \beta_j) g_t = (1 - \beta_j) \sum_{\tau=0}^t \beta_j^{t-\tau} g_\tau.$$

Using this and the definition of the average iterates, we have

$$\begin{aligned}
z_t^j - x_t^j &= \frac{\beta_j}{1 - \beta_j} (x_t^j - x_{t-1}^j) = -\frac{\eta \beta_j}{1 - \beta_j} u_t^j = -\eta \beta_j \sum_{\tau=0}^t \beta_j^{t-\tau} g_\tau \\
z_t - x_t &= \mathbb{E}_j [z_t^j - x_t^j] = \mathbb{E}_j \left[-\eta \beta_j \sum_{\tau=0}^t \beta_j^{t-\tau} g_\tau \right] = -\eta \sum_{\tau=0}^t \mathbb{E}_j [\beta_j^{t-\tau+1}] g_\tau \\
&= -\eta \sum_{\tau=0}^t \beta_\omega^{(t-\tau+1)} g_\tau, \quad \text{where } \beta_\omega^{(\tau)} = \mathbb{E}_j [\beta_j^\tau] = \sum_{j=1}^N \omega_j \beta_j^\tau.
\end{aligned}$$

Let us make another notation for the sum of weights in the above sum and bound it as follows:

$$\begin{aligned}
s_t &\stackrel{\text{def}}{=} \sum_{\tau=0}^t \beta_\omega^{(t-\tau+1)} = \sum_{\tau=0}^t \sum_{j=1}^N \omega_j \beta_j^{t-\tau+1} \\
&= \sum_{j=1}^N \omega_j \sum_{\tau=0}^t \beta_j^{t-\tau+1} = \sum_{j=1}^N \omega_j \frac{\beta_j - \beta_j^{t+2}}{1 - \beta_j} \leq \sum_{j=1}^N \frac{\omega_j \beta_j}{1 - \beta_j} \stackrel{\text{def}}{=} \beta_\omega.
\end{aligned}$$

Using convexity of squared norm, we have

$$\|z_t - x_t\|^2 = \eta^2 s_t^2 \left\| \sum_{\tau=0}^t \frac{\beta_\omega^{(t-\tau+1)}}{s_t} g_\tau \right\|^2 \leq \eta^2 s_t^2 \sum_{\tau=0}^t \frac{\beta_\omega^{(t-\tau+1)}}{s_t} \|g_\tau\|^2 \leq \eta^2 \beta_\omega \sum_{\tau=0}^t \beta_\omega^{(t-\tau+1)} \|g_\tau\|^2$$

Summing over the iterates yields

$$\begin{aligned}
\sum_{t=0}^{T-1} \mathbb{E} \|z_t - x_t\|^2 &\leq \eta^2 \beta_\omega \sum_{t=0}^{T-1} \sum_{\tau=0}^t \beta_\omega^{(t-\tau+1)} \mathbb{E} \|g_\tau\|^2 \\
&= \eta^2 \beta_\omega \sum_{\tau=0}^{T-1} \sum_{t=\tau}^{T-1} \beta_\omega^{(t-\tau+1)} \mathbb{E} \|g_\tau\|^2 = \eta^2 \beta_\omega \sum_{\tau=0}^{T-1} \left(\sum_{t=1}^{T-\tau} \beta_\omega^{(t)} \right) \mathbb{E} \|g_\tau\|^2 \\
&= \eta^2 \beta_\omega \sum_{\tau=0}^{T-1} \left(\sum_{j=1}^N \omega_j \frac{\beta_j - \beta_j^{T-\tau+1}}{1 - \beta_j} \right) \mathbb{E} \|g_\tau\|^2 \\
&\leq \eta^2 \beta_\omega^2 \sum_{\tau=0}^{T-1} \mathbb{E} \|g_\tau\|^2 \\
&= \eta^2 \beta_\omega^2 \sum_{\tau=0}^{T-1} \mathbb{E} \left\| \frac{1}{M} \sum_{m=1}^M g_\tau^m - \nabla f_m(x_\tau^m) \right\|^2 + \eta^2 \beta_\omega^2 \sum_{\tau=0}^{T-1} \mathbb{E} \left\| \frac{1}{M} \sum_{m=1}^M \nabla f_m(x_\tau^m) \right\|^2 \\
&= \frac{\eta^2 \beta_\omega^2}{M^2} \sum_{\tau=0}^{T-1} \sum_{m=1}^M \mathbb{E} \|g_\tau^m - \nabla f_m(x_\tau^m)\|^2 + \eta^2 \beta_\omega^2 \sum_{\tau=0}^{T-1} \mathbb{E} \left\| \frac{1}{M} \sum_{m=1}^M \nabla f_m(x_\tau^m) \right\|^2 \\
&= \frac{\eta^2 \beta_\omega^2}{M} T \sigma^2 + \eta^2 \beta_\omega^2 \sum_{\tau=0}^{T-1} \mathbb{E} \left\| \frac{1}{M} \sum_{m=1}^M \nabla f_m(x_\tau^m) \right\|^2.
\end{aligned}$$

□

Lemma 3. *If $24\eta^2 L^2 \psi \leq 1$, then*

$$\frac{1}{MT} \sum_{t=0}^{T-1} \sum_{m=1}^M \mathbb{E} \|x_t - x_t^m\|^2 \leq 12\eta^2 (B^2 - 1) \psi \cdot \frac{1}{T} \sum_{t=0}^{T-1} \mathbb{E} \|\nabla f(x_t)\|^2 + 4\eta^2 \psi (\sigma^2 + 3G^2),$$

where

$$\psi = \frac{4(1 - p_x)}{p_x^2} \cdot \sum_{j=1}^N \omega_j \frac{(1 - \beta_j)(1 - p_j)}{1 - (1 - p_j)\beta_j}$$

Proof. Let us expand the term $\mathbb{E} \|x_{t+1} - x_{t+1}^m\|^2$ using x_{t+1}^m 's probabilistic update rule:

$$\begin{aligned}
\mathbb{E} \|x_{t+1} - x_{t+1}^m\|^2 &= p_x \cdot 0 + (1 - p_x) \cdot \mathbb{E} \|x_t - \eta u_t - (x_t^m - \eta u_t^m)\|^2 \\
&= (1 - p_x) \cdot \mathbb{E} \|x_t - x_t^m - \eta(u_t - u_t^m)\|^2 \\
&\leq (1 - p_x)(1 + s) \mathbb{E} \|x_t - x_t^m\|^2 + \eta^2 (1 - p_x)(1 + 1/s) \mathbb{E} \|u_t - u_t^m\|^2 \\
&\leq \eta^2 (1 - p_x)(1 + 1/s) \sum_{\tau=1}^t ((1 - p_x)(1 + s))^{t-\tau} \mathbb{E} \|u_\tau - u_\tau^m\|^2.
\end{aligned}$$

where $s > 0$ will be chosen later. Next we expand the term $\mathbb{E}\|u_t^j - u_t^{j,m}\|^2$ using $u_t^{j,m}$'s probabilistic update rule:

$$\begin{aligned}
\mathbb{E}\|u_t^j - u_t^{j,m}\|^2 &= p_j \cdot 0 + (1 - p_j) \cdot \mathbb{E} \left\| \frac{1}{M} \sum_{m=1}^M (\beta_j u_{t-1}^{j,m} + (1 - \beta_j) g_{t-1}^m) - (\beta_j u_{t-1}^j + (1 - \beta_j) g_{t-1}^m) \right\|^2 \\
&= (1 - p_j) \mathbb{E} \left\| \beta_j (u_{t-1}^j - u_{t-1}^{j,m}) + (1 - \beta_j) (g_{t-1} - g_{t-1}^m) \right\|^2 \\
&\leq (1 - p_j) \beta_j \mathbb{E} \|u_{t-1}^j - u_{t-1}^{j,m}\|^2 + (1 - p_j) (1 - \beta_j) \mathbb{E} \|g_{t-1} - g_{t-1}^m\|^2 \\
&\leq (1 - p_j) (1 - \beta_j) \sum_{\tau=0}^{t-1} ((1 - p_j) \beta_j)^{t-\tau-1} \mathbb{E} \|g_\tau - g_\tau^m\|^2 \\
\mathbb{E}\|u_t - u_t^m\|^2 &\leq \sum_{j=1}^N \omega_j \mathbb{E} \|u_t^j - u_t^{j,m}\|^2 \\
&\leq \sum_{j=1}^N \omega_j (1 - p_j) (1 - \beta_j) \sum_{\tau=0}^{t-1} ((1 - p_j) \beta_j)^{t-\tau-1} \mathbb{E} \|g_\tau - g_\tau^m\|^2 \\
&\leq \sum_{\tau=0}^{t-1} \left(\sum_{j=1}^N \omega_j (1 - p_j) (1 - \beta_j) ((1 - p_j) \beta_j)^{t-\tau-1} \right) \mathbb{E} \|g_\tau - g_\tau^m\|^2 \\
&\leq \sum_{\tau=0}^{t-1} \left(\sum_{j=1}^N \omega_j (1 - p_j) (1 - \beta_j) q_j^{t-\tau-1} \right) \mathbb{E} \|g_\tau - g_\tau^m\|^2.
\end{aligned}$$

Denote $q_x = (1 - p_x)(1 + s)$, $q'_x = (1 - p_x)(1 + 1/s)$ and $q_j = (1 - p_j)\beta_j$. Combining the previous two bounds, we get

$$\begin{aligned}
&\frac{1}{M} \sum_{m=1}^M \mathbb{E} \|x_t - x_t^m\|^2 \\
&\leq \eta^2 q'_x \sum_{\tau=1}^t q_x^{t-\tau} \frac{1}{M} \sum_{m=1}^M \mathbb{E} \|u_\tau - u_\tau^m\|^2 \tag{4} \\
&\leq \eta^2 q'_x \sum_{\tau=1}^t q_x^{t-\tau} \frac{1}{M} \sum_{m=1}^M \sum_{\nu=0}^{\tau-1} \left(\sum_{j=1}^N \omega_j (1 - p_j) (1 - \beta_j) q_j^{\tau-\nu-1} \right) \mathbb{E} \|g_\nu - g_\nu^m\|^2 \\
&= \eta^2 q'_x \sum_{j=1}^N \omega_j (1 - p_j) (1 - \beta_j) \sum_{\tau=1}^t \sum_{\nu=0}^{\tau-1} q_x^{t-\tau-1} q_j^{\tau-\nu} \left[\frac{1}{M} \sum_{m=1}^M \mathbb{E} \|g_\nu - g_\nu^m\|^2 \right] \\
&= \eta^2 q'_x \sum_{j=1}^N \omega_j (1 - p_j) (1 - \beta_j) \sum_{\nu=0}^{t-1} \sum_{\tau=\nu+1}^t q_x^{t-\tau} q_j^{\tau-\nu-1} \left[\frac{1}{M} \sum_{m=1}^M \mathbb{E} \|g_\nu - g_\nu^m\|^2 \right] \\
&= \eta^2 q'_x \sum_{j=1}^N \omega_j (1 - p_j) (1 - \beta_j) \sum_{\nu=0}^{t-1} \frac{q_x^{t-\nu} - q_j^{t-\nu}}{q_x - q_j} \left[\frac{1}{M} \sum_{m=1}^M \mathbb{E} \|g_\nu - g_\nu^m\|^2 \right], \\
&= \eta^2 q'_x \sum_{j=1}^N \omega_j (1 - \beta_j) (1 - p_j) \sum_{\nu=0}^{t-1} \frac{q_x^{t-\nu} - q_j^{t-\nu}}{q_x - q_j} \left[\frac{1}{M} \sum_{m=1}^M \mathbb{E} \|g_\nu - g_\nu^m\|^2 \right], .
\end{aligned}$$

Next, we bound the gradient term above.

$$\begin{aligned}
\frac{1}{M} \sum_{m=1}^M \mathbb{E} \|g_t^m - g_t\|^2 &= \frac{1}{M} \sum_{m=1}^M \mathbb{E} \left\| g_t^m - \frac{1}{M} \sum_{i=1}^M g_t^i \right\|^2 \\
&\leq \frac{2}{K} \sum_{m=1}^M \mathbb{E} \left\| g_t^m - \nabla f_m(x_t^m) - \frac{1}{M} \sum_{i=1}^M (g_t^i - \nabla f_i(x_t^i)) \right\|^2 \\
&\quad + \frac{2}{M} \sum_{m=1}^M \mathbb{E} \left\| \nabla f_m(x_t^m) - \frac{1}{M} \sum_{i=1}^M \nabla f_i(x_t^i) \right\|^2 \\
(\text{Lemma 4}) &\leq \frac{2}{M} \sum_{m=1}^M \mathbb{E} \|g_t^m - \nabla f_m(x_t^m)\|^2 - 2\mathbb{E} \left\| \frac{1}{M} \sum_{m=1}^M (g_t^m - \nabla f_m(x_t^m)) \right\|^2 \\
&\quad + \frac{12L^2}{M} \sum_{m=1}^M \mathbb{E} \|x_t - x_t^m\|^2 + 6(B^2 - 1)\mathbb{E} \|\nabla f(x_t)\|^2 + 6G^2 \\
&\leq 2\sigma^2 + \frac{12L^2}{M} \sum_{m=1}^M \mathbb{E} \|x_t - x_t^m\|^2 + 6(B^2 - 1)\mathbb{E} \|\nabla f(x_t)\|^2 + 6G^2.
\end{aligned}$$

Averaging over the iterates and plugging this bound to the previous one, we get

$$\begin{aligned}
&\frac{1}{MT} \sum_{t=0}^{T-1} \sum_{m=1}^M \mathbb{E} \|x_t - x_t^m\|^2 \\
&\leq \frac{1}{MT} \sum_{t=1}^T \sum_{m=1}^M \mathbb{E} \|x_t - x_t^m\|^2 \\
&\leq \frac{\eta^2 q'_x}{T} \sum_{j=1}^N \omega_j (1 - \beta_j) (1 - p_j) \sum_{t=1}^T \sum_{\tau=0}^{t-1} \frac{q_x^{t-\tau} - q_j^{t-\tau}}{q_x - q_j} \left[\frac{1}{M} \sum_{m=1}^M \mathbb{E} \|g_\tau - g_\tau^m\|^2 \right] \\
&= \frac{\eta^2 q'_x}{T} \sum_{j=1}^N \omega_j (1 - \beta_j) (1 - p_j) \sum_{\tau=0}^{T-1} \sum_{t=\tau+1}^T \frac{q_x^{t-\tau} - q_j^{t-\tau}}{q_x - q_j} \left[\frac{1}{M} \sum_{m=1}^M \mathbb{E} \|g_\tau - g_\tau^m\|^2 \right] \\
&= \frac{\eta^2 q'_x}{T} \sum_{j=1}^N \frac{\omega_j (1 - \beta_j) (1 - p_j)}{q_x - q_j} \sum_{\tau=0}^{T-1} \left(\frac{q_x (1 - q_x^{T-\tau})}{1 - q_x} - \frac{q_j (1 - q_j^{T-\tau})}{1 - q_j} \right) \left[\frac{1}{M} \sum_{m=1}^M \mathbb{E} \|g_\tau - g_\tau^m\|^2 \right] \\
&\leq \frac{\eta^2 q'_x}{T} \sum_{j=1}^N \frac{\omega_j (1 - \beta_j) (1 - p_j)}{q_x - q_j} \sum_{\tau=0}^{T-1} \left(\frac{q_x}{1 - q_x} - \frac{q_j}{1 - q_j} \right) \left[\frac{1}{M} \sum_{m=1}^M \mathbb{E} \|g_\tau - g_\tau^m\|^2 \right] \\
&= \frac{\eta^2 q'_x}{T} \sum_{j=1}^N \frac{\omega_j (1 - \beta_j) (1 - p_j)}{(1 - q_x)(1 - q_j)} \sum_{\tau=0}^{T-1} \left[\frac{1}{M} \sum_{m=1}^M \mathbb{E} \|g_\tau - g_\tau^m\|^2 \right]
\end{aligned}$$

Now, let us optimize the factor

$$\frac{q'_x}{1 - q_x} = \frac{(1 - p_x)(1 + 1/s)}{1 - (1 - p_x)(1 + s)}$$

by choosing optimal value for s introduced earlier. By the first order optimality condition, we find that the optimal value is $s^* = \frac{1}{\sqrt{1-p_x}} - 1$. Hence, the minimal value of the factor is

$$\begin{aligned}
\frac{q'_x}{1 - q_x} &= \frac{1 - p_x}{(1 - \sqrt{1 - p_x})^2} \\
&= \frac{(1 - p_x)(1 - \sqrt{1 - p_x})^2}{(1 - \sqrt{1 - p_x})^2(1 + \sqrt{1 - p_x})^2} = \frac{(1 - p_x)(1 + \sqrt{1 - p_x})^2}{p_x^2} \leq \frac{4(1 - p_x)}{p_x^2}.
\end{aligned}$$

Letting

$$\psi = \frac{4(1-p_x)}{p_x^2} \sum_{j=1}^N \omega_j \frac{(1-\beta_j)(1-p_j)}{1-q_j} = \frac{4(1-p_x)}{p_x^2} \sum_{j=1}^N \omega_j \frac{(1-\beta_j)(1-p_j)}{1-(1-p_j)\beta_j}$$

and continuing the chain of bounds, we get

$$\begin{aligned} & \frac{1}{MT} \sum_{t=0}^{T-1} \sum_{m=1}^M \mathbb{E} \|x_t - x_t^m\|^2 \\ & \leq \eta^2 \psi \cdot \frac{1}{T} \sum_{t=0}^{T-1} \left[\frac{1}{K} \sum_{m=1}^M \mathbb{E} \|g_t - g_t^m\|^2 \right] \\ & \leq \eta^2 \psi \cdot \frac{1}{T} \sum_{t=0}^{T-1} \left[\frac{12L^2}{M} \sum_{m=1}^M \mathbb{E} \|x_t - x_t^m\|^2 + 6(B^2 - 1) \mathbb{E} \|\nabla f(x_t)\|^2 + 2\sigma^2 + 6G^2 \right] \\ & \leq 12\eta^2 L^2 \psi \cdot \frac{1}{TM} \sum_{t=0}^{T-1} \sum_{m=1}^M \mathbb{E} \|x_t - x_t^m\|^2 \\ & \quad + 6\eta^2 (B^2 - 1) \psi \cdot \frac{1}{T} \sum_{t=0}^{T-1} \mathbb{E} \|\nabla f(x_t)\|^2 + 2\eta^2 \psi (\sigma^2 + 3G^2). \end{aligned}$$

Assuming $12\eta^2 L^2 \psi \leq 1/2$ and reordering the first term in the bound, we arrive

$$\frac{1}{MT} \sum_{t=0}^{T-1} \sum_{m=1}^M \mathbb{E} \|x_t - x_t^m\|^2 \leq 12\eta^2 (B^2 - 1) \psi \cdot \frac{1}{T} \sum_{t=0}^{T-1} \mathbb{E} \|\nabla f(x_t)\|^2 + 4\eta^2 \psi (\sigma^2 + 3G^2).$$

□

Lemma 4. *Under smoothness and bounded heterogeneity assumptions 1 and 3, we have*

$$\frac{1}{M} \sum_{m=1}^M \left\| \nabla f_m(y^m) - \frac{1}{K} \sum_{i=1}^K \nabla f_i(y^i) \right\|^2 \leq \frac{6L^2}{M} \sum_{m=1}^M \|y - y^m\|^2 + 3(B^2 - 1) \|\nabla f(y)\|^2 + 3G^2,$$

for any $y^1, \dots, y^m \in \mathbb{R}^d$ and $y = \mathbb{E}_m[y^m]$.

Proof. The proof follows from Lemma 5 of [19] as the result does not depend on the optimizer. □

E Wall-Clock Time Modeling

To assess the practical benefits of our proposal, we analyze its impact on total wall-clock time by modeling two distinct synchronization strategies: a simple unified frequency approach and a desynchronized approach based on optimizer state half-lives. We adopt the model from DES-LOC [19] for estimating total training time.

E.1 Wall-Clock Time Model

The total wall-clock time is modeled as the sum of computational and communication time: $t_{\text{total}} = t_{\text{compute}} + t_{\text{comms}}$. The computation time, t_{compute} , is a function of model and dataset size, while the communication time, t_{comms} , depends on the number and size of synchronization events.

For a training process of T total steps, the communication time for an AllReduce operation [50] depends on the payload size, number of workers M , bandwidth B , and latency l . The total time for different methods and strategies is:

Unified Frequency Methods: Parameters and all optimizer states are synchronized together every K steps. The total payload is $3d$ (for parameters, first and second momenta). This applies to Local Adam and a baseline version of our method, MT-DAO (Unified).

$$t_{\text{total,Unified}} = t_{\text{compute}} + \frac{T}{K} \cdot \left[\frac{2(3d)}{B} \left(1 - \frac{1}{M} \right) + l \right] \quad (5)$$

Half-Life Based Methods: Parameters (K_x), first momentum (K_u), and second momentum (K_v) are synchronized at different frequencies. This applies to DES-LOC and our proposed method, MT-DAO (Half-Life).

$$t_{\text{total,Half-Life}} = t_{\text{compute}} + \left(\frac{T}{K_x} + \frac{T}{K_u} + \frac{T}{K_v} \right) \cdot \left[\frac{2d}{B} \left(1 - \frac{1}{M} \right) + l \right] \quad (6)$$

Limitation: This model does not account for any potential overlap between computation and communication.

E.2 Experimental Configuration

We compare the two synchronization strategies. The **Unified Frequency** strategy serves as a baseline, where all states are synchronized together every $K_x = 32$ steps. This includes Local Adam, Local ADOPT, and a variant of our method, MT-DAO (Unified), which uses a high β_1 value but is forced to sync at the same frequent rate as its parameters. These methods have equivalent communication costs and will overlap for an iso-token budget, however, the results in Section 5 show that MT-DAO achieves the same perplexity as Local ADOPT in many fewer optimization steps, outperforming on time-to-perplexity metrics.

The **Half-Life Based** strategy aims to improve efficiency by synchronizing states less frequently if they change slowly. The synchronization frequency is set based on the state’s half-life, $\tau_{0.5}(\beta) = \ln(0.5)/\ln(\beta)$. This includes DES-LOC and MT-DAO (Half-Life). The quasi-hyperbolic (QH) configuration of MT-DAO allows it to use an extremely high $\beta_1 = 0.999$, leading to a very long half-life and thus a much lower communication frequency for its first momentum. We use $\beta_2 = 0.999$ for ADAM variants and $\beta_2 = 0.9999$ for ADOPT variants.

Table 3 details the configurations for both strategies.

Table 3: Hyperparameter configurations and synchronization frequencies (K) for modeled methods, grouped by synchronization strategy. For the Half-Life strategy, momentum frequencies are set to the closest power of two to their half-life.

Strategy	Method	ω Values	β_1 Values	β_2 Value	Sync Freq. K_{u_1}	Sync Freq. K_v
<i>Unified Frequency (All states sync every $K_x = 32$ steps)</i>						
Unified	Local Adam	N/A	{0.95}	0.99	32	32
Unified	Local ADOPT	N/A	{0.95}	0.9999	32	32
Unified	MT-DAO-Adam (Unified)	{0.95}	{0.999}	0.999	32	32
Unified	MT-DAO-ADOPT (Unified)	{0.95}	{0.999}	0.9999	32	32
<i>Half-Life Based Frequency (States sync at different rates from $K_x = 32$)</i>						
Half-Life	DES-LOC-ADAM	N/A	{0.95}	0.99	32	69
Half-Life	DES-LOC-ADOPT	N/A	{0.95}	0.9999	32	6931
Half-Life	MT-DAO-Adam (Half-Life)	{0.95}	{0.999}	0.999	693	693
Half-Life	MT-DAO-ADOPT (Half-Life)	{0.95}	{0.999}	0.9999	693	6931

E.3 Modeling Results

The following figures present the estimated wall-clock time and communication costs when training a 1B model on 4 H100 machines with a batch size of 2M tokens and sequence length of 2048. The results demonstrate that MT-DAO significantly reduces communication cost with both strategies, with the half-life one being generally more effective.

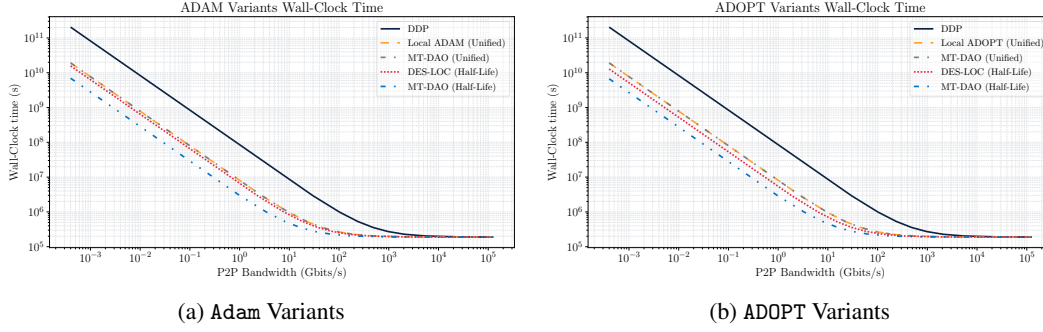


Figure 9: Estimated total wall-clock time as a function of interconnect bandwidth. For both (a) Adam and (b) ADOPT, methods using the Half-Life strategy outperform those using a Unified frequency.

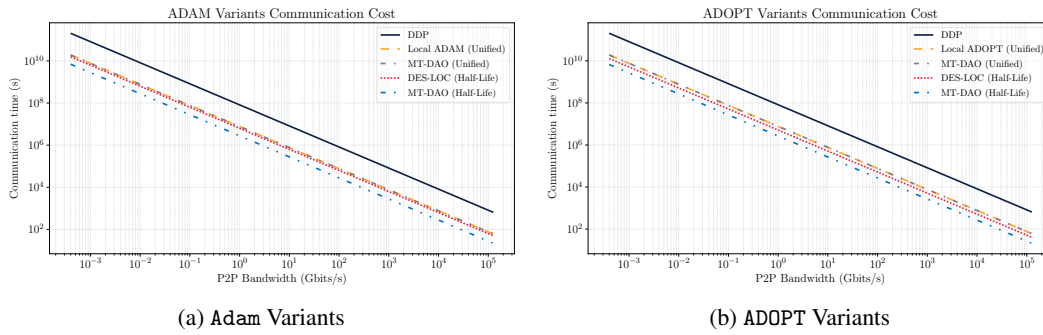


Figure 10: Estimated total communication time. The plots clearly distinguish the two strategies. The Unified frequency methods (Local Adam and MT-DAO (Unified)) have identical high costs. The Half-Life methods are more efficient, with MT-DAO (Half-Life) being the most efficient due to its ability to leverage a high- β momentum that requires infrequent updates.

Takeaway: MT-DAO can significantly reduce communication costs across bandwidths.

F Derivations of Mutual Information and Variance

This section provides the detailed derivations for the expressions referenced in the main text.

F.1 Variance of Local Momentum

The variance of the final local momentum, $\text{Var}(u_{t+K})$, is derived under the assumption that the stochastic gradients g_t are independent and identically distributed random variables with variance σ_m^2 .

The unrolled momentum update over K local steps is given by:

$$u_{t+K} = \beta^K u_t + (1 - \beta) \sum_{k=0}^{K-1} \beta^k g_{t+K-k}$$

The variance is calculated with respect to the randomness in the local gradients $\{g_{t+1}, \dots, g_{t+K}\}$. The initial momentum u_t is treated as a constant, as it is a synchronized state before local updates begin.

Applying the variance operator:

$$\text{Var}(u_{t+K}) = \text{Var} \left(\beta^K u_t + (1 - \beta) \sum_{k=0}^{K-1} \beta^k g_{t+K-k} \right)$$

Since u_t is constant, $\text{Var}(\beta^K u_t) = 0$. Using the property $\text{Var}(aX) = a^2 \text{Var}(X)$:

$$\text{Var}(u_{t+K}) = (1 - \beta)^2 \text{Var} \left(\sum_{k=0}^{K-1} \beta^k g_{t+K-k} \right)$$

Given the assumption that the gradients g_{t+i} are independent, the variance of their weighted sum is the weighted sum of their variances, where weights are squared:

$$\text{Var} \left(\sum_{k=0}^{K-1} \beta^k g_{t+K-k} \right) = \sum_{k=0}^{K-1} \text{Var}(\beta^k g_{t+K-k}) = \sum_{k=0}^{K-1} (\beta^k)^2 \text{Var}(g_{t+K-k})$$

Assuming each local gradient has variance σ_m^2 :

$$\text{Var} \left(\sum_{k=0}^{K-1} \beta^k g_{t+K-k} \right) = \sum_{k=0}^{K-1} \beta^{2k} \sigma_m^2 = \sigma_m^2 \sum_{k=0}^{K-1} (\beta^2)^k$$

The summation is a finite geometric series, $\sum_{i=0}^{n-1} r^i = \frac{1-r^n}{1-r}$. With $r = \beta^2$ and $n = K$:

$$\sum_{k=0}^{K-1} (\beta^2)^k = \frac{1 - (\beta^2)^K}{1 - \beta^2} = \frac{1 - \beta^{2K}}{1 - \beta^2}$$

Substituting this back into the expression for $\text{Var}(u_{t+K})$:

$$\text{Var}(u_{t+K}) = (1 - \beta)^2 \sigma_m^2 \frac{1 - \beta^{2K}}{1 - \beta^2}$$

By factoring the denominator $1 - \beta^2 = (1 - \beta)(1 + \beta)$, we can simplify the expression:

$$\text{Var}(u_{t+K}) = (1 - \beta)^2 \sigma_m^2 \frac{1 - \beta^{2K}}{(1 - \beta)(1 + \beta)} = \frac{1 - \beta}{1 + \beta} (1 - \beta^{2K}) \sigma_m^2$$

This completes the derivation.

F.2 Mutual Information

The mutual information $I(U_{t+K}; U_t)$ is derived by modeling the momentum states as multivariate Gaussian random vectors. The model for the update process is:

$$U_{t+K} = \beta^K U_t + L$$

The following assumptions are made:

1. The initial momentum U_t is a Gaussian random vector with zero mean and covariance Σ_{U_t} , i.e., $U_t \sim \mathcal{N}(0, \Sigma_{U_t})$.
2. The accumulated local gradient noise L is a Gaussian random vector with zero mean and covariance Σ_L , i.e., $L \sim \mathcal{N}(0, \Sigma_L)$.
3. U_t and L are statistically independent.

The mutual information between two random vectors X and Y is defined as $I(X; Y) = h(Y) - h(Y|X)$, where $h(\cdot)$ is the differential entropy. For a d -dimensional Gaussian vector $Z \sim \mathcal{N}(\mu, \Sigma)$, the entropy is $h(Z) = \frac{1}{2} \log \det(2\pi e \Sigma)$.

First, we determine the distribution of U_{t+K} . As a linear combination of independent Gaussian vectors, it is also Gaussian.

- **Mean:** $\mathbb{E}[U_{t+K}] = \mathbb{E}[\beta^K U_t + L] = \beta^K \mathbb{E}[U_t] + \mathbb{E}[L] = 0$.
- **Covariance:** $\text{Cov}(U_{t+K}) = \text{Cov}(\beta^K U_t + L)$. Due to the independence of U_t and L :

$$\Sigma_{U_{t+K}} = \text{Cov}(\beta^K U_t) + \text{Cov}(L) = \beta^{2K} \Sigma_{U_t} + \Sigma_L$$

Thus, $U_{t+K} \sim \mathcal{N}(0, \beta^{2K}\Sigma_{U_t} + \Sigma_L)$.

The entropy of U_{t+K} is:

$$h(U_{t+K}) = \frac{1}{2} \log \det (2\pi e(\beta^{2K}\Sigma_{U_t} + \Sigma_L))$$

Next, we determine the conditional entropy $h(U_{t+K}|U_t)$. The distribution of U_{t+K} conditioned on a specific value $U_t = u_t$ is:

$$U_{t+K}|U_t = u_t \sim \mathcal{N}(\beta^K u_t, \Sigma_L)$$

The entropy of this conditional distribution is:

$$h(U_{t+K}|U_t = u_t) = \frac{1}{2} \log \det(2\pi e\Sigma_L)$$

Since this expression does not depend on the specific value u_t , the conditional entropy $h(U_{t+K}|U_t)$ is the same.

Now, we compute the mutual information:

$$\begin{aligned} I(U_{t+K}; U_t) &= h(U_{t+K}) - h(U_{t+K}|U_t) \\ I(U_{t+K}; U_t) &= \frac{1}{2} \log \det (2\pi e(\beta^{2K}\Sigma_{U_t} + \Sigma_L)) - \frac{1}{2} \log \det(2\pi e\Sigma_L) \end{aligned}$$

Using the logarithmic property $\log a - \log b = \log(a/b)$:

$$I(U_{t+K}; U_t) = \frac{1}{2} \log \left(\frac{\det(2\pi e(\beta^{2K}\Sigma_{U_t} + \Sigma_L))}{\det(2\pi e\Sigma_L)} \right)$$

The constant factors $(2\pi e)^d$ cancel out. Using the determinant property $\frac{\det(A)}{\det(B)} = \det(AB^{-1})$:

$$I(U_{t+K}; U_t) = \frac{1}{2} \log \det ((\beta^{2K}\Sigma_{U_t} + \Sigma_L)\Sigma_L^{-1})$$

Distributing Σ_L^{-1} inside the determinant:

$$I(U_{t+K}; U_t) = \frac{1}{2} \log \det (\beta^{2K}\Sigma_{U_t}\Sigma_L^{-1} + \Sigma_L\Sigma_L^{-1})$$

$$I(U_{t+K}; U_t) = \frac{1}{2} \log \det (I + \beta^{2K}\Sigma_{U_t}\Sigma_L^{-1})$$

This completes the derivation.

G Extended Related Work

Strategies for Communication-Efficient Distributed Training. A substantial body of research aims to curtail communication overhead in distributed training, primarily by either reducing the frequency of synchronizations or compressing the data transmitted per round. The first approach, often termed periodic or local SGD, involves performing multiple local optimization steps between global aggregations. This strategy has been extensively analyzed in both IID and non-IID contexts (see Kairouz et al. [21] for a survey and Lin et al. [31]). In the realm of foundation-model pre-training, methods like **DiLoCo** [7] have shown that infrequent synchronization can, with careful tuning, achieve performance comparable to or better than standard data parallelism, with scaling laws characterizing its behavior across model sizes [7]. This paradigm has also been adapted for federated-style pre-training [46] and variants with overlapping or eager updates [13, 22]. The second strategy involves compressing communication payloads. Techniques range from randomized quantization (**QSGD**) [2] and sparse updates tailored for non-IID data (**STC**, **ZeroFL**) [47, 42] to one-bit aggregation (**signSGD-MV**) [6]. In practice, these two strategies are often combined; for instance, **FedPAQ** integrates local training with quantization and partial participation to provide strong theoretical guarantees [44].

Multi-Timescale Momentum for Temporal Mismatches. The temporal discrepancy between frequent local updates and infrequent global synchronizations creates a need for optimizers that can integrate information across different timescales. Standard momentum, while beneficial in low-curvature landscapes [53], imposes a compromise: low decay values are responsive but slow, whereas high decay values are fast but prone to oscillations [36]. A single exponential moving average (EMA) cannot effectively weight both recent and distant gradients [40]. Multi-timescale optimizers address this limitation. **Quasi-Hyperbolic Momentum (QHM)** decouples the current gradient’s weight from the momentum decay rate (β) [37], recovering methods like Nesterov and Triple Momentum [48]. **Aggregated Momentum (AggMo)** maintains and averages multiple momentum buffers with distinct β values, using faster-decaying terms to passively damp oscillations caused by slower, more aggressive terms [36]. Similarly, **AdEMAMix** mixes a fast EMA with an ultra-slow one (e.g., $\beta_3 = 0.9999$), demonstrating that long-term gradient memory significantly reduces catastrophic forgetting in language models [40]. This principle of leveraging multiple timescales is also present in other contexts. Optimizers like Grokfast [27] and AdMeta [9] employ nested EMAs for different purposes, providing orthogonal evidence for the value of long-term momentum. While these methods have shown promise in step-wise synchronous training, their potential to resolve the temporal mismatch in communication-efficient distributed optimization remains largely unexplored.

Perspectives from Federated Optimization. The field of Federated Learning (FL), particularly in the cross-device setting, offers a rich history of methods for managing statistical heterogeneity and communication constraints, which are central challenges. The foundational **FedAvg** algorithm [39] has inspired numerous successors (see survey by Kairouz et al. [21]). To counteract *client drift* caused by non-IID data, **FedProx** introduces a proximal regularizer for stability [29], **SCAFFOLD** employs control variates to reduce gradient variance [24], and **FedNova** normalizes local updates to correct for objective inconsistency [55]. Server-side momentum (**FedAvgM**) has also been shown to stabilize aggregation under data skew [17]. Adaptive methods have been extended to this setting in **Adaptive Federated Optimization (FEDOPT)**, which provides nonconvex guarantees for *FedAdam*, *FedYogi*, and *FedAdagrad* [26]. Furthermore, **Mime** adapts centralized algorithms to FL by marrying control variates with server statistics [23]. Personalization techniques, such as meta-learning-based **Per-FedAvg** [14] and **FedL2P** [28] or the regularized **Ditto** [30], complement these global models by improving per-client utility.

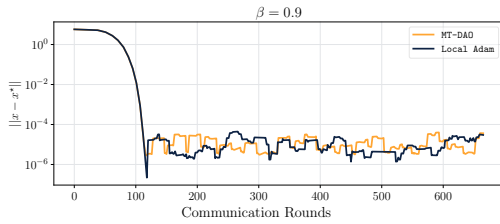
Orthogonal Approaches in Payload Compression and Optimizer Design. Orthogonal to reducing synchronization frequency, another line of work focuses on compressing the communication payload itself, often in combination with periodic training. Foundational methods include quantization, as in **QSGD** [2], and sparsification, as in **Deep Gradient Compression** [32], with convergence analyses providing theoretical grounding [3]. More recent work like **CocktailSGD** combines random and top- k sparsification with quantization for aggressive compression during LLM fine-tuning [57]. Beyond compressing gradients, some methods compress the optimizer *states*. For instance, **LDAdam** performs adaptive updates using low-rank approximations of gradient statistics [45], while **DeMo** decouples momentum across workers and communicates only selected components [41]. Other advanced optimizers aim for stability and efficiency through different mechanisms; for example, **Lion** uses a sign function with interpolated momentum [8], and **Sophia** employs a Hessian-based pre-conditioner to temper step sizes in high-curvature directions [33]. These approaches are generally compatible with and can be composed with infrequent synchronization strategies.

H Additional Results

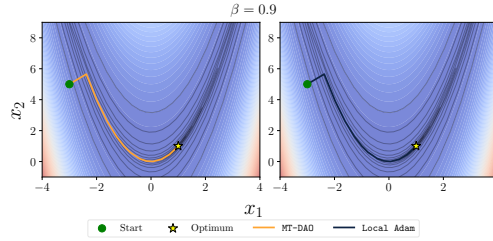
To investigate the stability of MT-DAO under varied momentum parameterizations, we now examine its performance in a fast β regime. Figure 11 presents the results of this comparison, plotting both the convergence rate in terms of distance to the optimum and the optimization trajectories on the function’s contour plot.

I LLM Usage Declaration

As declared in the submission form, LLMs were used in this work in order to aid or polish writing and for retrieval and discovery of related work. We used GPT-5 and Gemini 2.5 PRO primarily to abbreviate or rephrase text or to evaluate the clarity of our writing and provide guidance on areas of



(a) Distance to optimum vs. steps.



(b) Contour plot of trajectories.

Figure 11: MT-DA0 remains stable in both fast β regimes, as pictured here, and in slow β regimes as in Figure 2. This is unlike prior stateful methods like Local Adam which only offer stable convergence for fast β values. As before, we optimize the non-convex Rosenbrock function $f(x_1, x_2) = (1 - x_1)^2 + 100(x_2 - x_1^2)^2$ with $M = 256$ workers and IID Gaussian noise ($\sigma = 2$).

improvement. We also used the deep research feature present in both models in order to discover, but not describe or interpret, additional papers for our extended literature review in Section G. Finally, we used both models to generate plotting code and as general code assistants.